Event Shape Dependence of Symmetry Plane Correlations in Pb-Pb Collisions at the LHC Energies using AMPT

A thesis

Submitted towards the partial fulfillment of

BS-MS Dual Degree programme

by

Sarthak Tripathy

Date: 23/04/2025

under the guidance of

Prof. Raghunath Sahoo

Indian Institute of Technology Indore

from May 2024 to March 2025

Indian Institute of Science Education and Research Pune

Certificate

This is to certify that this dissertation entitled **"Event Shape Dependence of Symmetry Plane Correlations in Pb-Pb Collisions at the LHC Energies using AMPT"** submitted towards the partial fulfillment of the BS-MS Dual Degree at the Indian Institute of Science Education and Research (IISER) Pune represents original research carried out by **Sarthak Tripathy** at the **Indian Institute of Technology Indore**, under the supervision of **Prof. Raghunath Sahoo** during academic year May 2024 to March 2025.

(Supervisor) 23/04/2025

RAGHUNATH SAHOO
PROFESSOR,
DEPARTMENT OF PHYSICS,
IIT INDORE

Dr. Raghunath Sahoo | डॉ. रघुनाथ साहू
Professor | प्राध्यापक
Department of Physics | भौतिकी विभाग
Indian Institute of Technology Indore, India
भारतीय प्रौद्योगिकी संस्थान इन्दौर, भारत

(TAC Member)

SEEMA SHARMA
PROFESSOR,
DEPARTMENT OF PHYSICS,
IISER PUNE

DATE: 23/04/2025

Declaration

I, hereby declare that the matter embodied in the report titled "**Event Shape Dependence of Symmetry Plane Correlations in Pb-Pb Collisions at the LHC Energies using AMPT**" is the result of the investigations carried out by me at the **Indian Institute of Technology Indore** from the period **17-05-2024** to **15-03-2025** under the supervision of **Prof. Raghunath Sahoo** and the same has not been submitted elsewhere for any other degree.

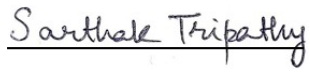

(Student)

Sarthak Tripathy

Roll No.: 20201115

Program: BS-MS

IISER Pune

Date: 23/04/2025

This thesis is dedicated to my parents, to all my teachers and guides so far.

Acknowledgements

Firstly, I would like to thank Prof. Raghunath Sahoo for supervising me well throughout the year I carried out this research project and showing me directions where progress could be made. I must also thank Prof. Seema Sharma for providing her valuable suggestions and carrying out necessary interrogations during meetings where I had to provide updates regarding my work progress.

This work could not have possibly progressed without the support from the seniors in the group of Prof. Sahoo. Among them, the most vital role was played by Mr. Suraj Prasad, who helped in formulating the problem, and by providing feedback and suggesting me improvements every time I presented the progress of my investigation. I would also like to thank Dr. C.R. Singh for very actively leading discussions regarding current topics, as well as historically, as to how physics is evolving and has evolved. He also has helped me in improving my theoretical understanding by providing me feedback on certain theoretical derivations that I carried out during my research project. A vital contribution to my understanding of concepts relevant to this work has been made by the thorough interrogations that were carried out by Mr. Bhagyarathi Sahoo at several points throughout this time. Fruitful discussions with Dr. Ronald Scaria guided me to streamline my work in an efficient way. Constant and encouraging interactions with Mr. Kamaljeet Singh helped me save a lot of time that could not have been possible otherwise. I must also express my gratitude towards Mr. Debadatta Behera, Mr. Kshitish K. Pradhan, Ms. Aswathy Menon, Mr. Kangkan Goswami, Ms. Purnima Srivastava and Ms. Parul Mittal for the insightful conversations that I had with them while having meals at the canteens of IIT Indore, that contributed to both my academic and non-academic thinking. I would especially like to thank Parul, whose active and friendly presence during the most challenging phase of time I had ever experienced, was of utmost help to me in navigating back to normalcy and continue my work in a steadfast manner. I shall cherish the time I spent with everyone who were involved with me during my stay at Indore, whether for a long, or even a short duration and cannot exhaustively complete the list of people I am thankful towards.

I acknowledge the computing facility provided by the Grid Computing Facility, VECC, Kolkata, India. This work could not have been carried out otherwise within the stipulated time. A significant portion of the cost of my stay at Indore, and also through all the four earlier years of my BS-MS Dual Degree career was borne by the KVPY scholarship.

Finally, I express gratitude towards my parents, for encouraging me to go along the path of my interest and pursue higher qualifications relevant to carrying out scientific research as my career, instead of pressurizing me to settle for a highly paying job. I would like to thank also, my teachers at IISER Pune, who very actively took to teaching the concepts and giving every possible effort that they could have for students to be trained well in the courses that they took.

Abstract

Anisotropy in final state particle emission in Pb-Pb collisions at $\sqrt{s_{\mathrm{NN}}}$ = 5.02 TeV is expected to arise as a consequence of anisotropy in energy distribution of the initial colliding system. This thesis aims to explore and comprehend the configuration of initial energy distribution using the correlations in symmetry plane angles corresponding to the anisotropy of final state particle emission in the transverse momentum space in Pb-Pb collisions at $\sqrt{s_{\mathrm{NN}}}$ = 5.02 TeV which have been generated using A Multi-Phase Transport (AMPT) model. The Gaussian Estimator (GE) has been used for the purpose of evaluating the symmetry plane correlations (SPCs), as it provides information unbiased of the fluctuations of the anisotropy from one event to the other. In analogy to the GE of SPCs, participant plane correlations (PPCs) have been defined, which characterize the geometry of the initial colliding region in a way very similar to how SPCs characterize final state transverse momentum distribution. In this geometrical context, it is suggestive to carry out an event shape differentiated study of the SPCs in order to gain a better understanding regarding them. The event shape classifier used for this purpose is transverse spherocity.

While most of the SPCs show striking contrast in different event shape classes, the PPCs show no such difference. Most of the SPCs exhibit qualitatively, the same centrality dependence as their corresponding PPCs. In this study, a linear relationship between some SPCs and their corresponding PPCs have been found in Pb-Pb collisions at the LHC energies, generated with AMPT. This work could find application by providing geometry based physical insight into the development of models using Bayesian analysis for deciding the best values of parameters, as each SPC and their corresponding PPC give unique information regarding the geometry of the respective states of the collision system that they are defined in.

Contents

List of Figures

List of Tables

Chapter 1

Introduction

1.1 The Standard Model

The Standard Model (SM) (Fig. 1.1) is the most widely accepted theory of fundamental particles and the interactions among them. It is a quantum field theory (QFT) with a gauge symmetry group $SU(3) \times SU(2) \times U(1)$. The SM consists of twelve spin-1/2 fermions which come in 3 generations of quarks, with 2 quarks in each generation; and 3 generations of leptons, with 2 leptons in each generation. In order to mediate the forces between these fermions, there are the vector bosons – the photon, the Z and the $W^{\pm}$ bosons - which mediate the electromagnetic and the weak (together referred to as the electroweak) interactions among all fermions; and eight types of gluons, which are carriers of the strong force between quarks. The SM also consists of the scalar boson Higgs, which is responsible for the masses of the fundamental particles. All fermions have their corresponding antiparticles. In addition to spin, the quarks have 3 color degrees of freedom.

1.2 Quantum Chromodynamics

The strong force is modeled using the QFT called Quantum Chromodynamics (QCD), which is the theory with the $SU(3)$ gauge symmetry group in the SM. The QCD Lagrangian is as follows [1]:

$$\mathcal{L} = \bar{q}(i\gamma^{\mu} D_{\mu} - m)q - \frac{1}{4} F^{a}_{\mu\nu} F^{\mu\nu a} \tag{1.1}$$

where

$$D_{\mu} = \partial_{\mu} - igA^{a}_{\mu} T^{a}$$
$$F^{a}_{\mu\nu} = \partial_{\mu} A^{a}_{\nu} - \partial_{\nu} A^{a}_{\mu} - g f^{abc} A^{b}_{\mu} A^{c}_{\nu}$$

where, q represents the color state of the quarks and $\bar{q}$ is dual to q. a is an index that runs from 1 to 8, for the 8 generators of the $SU(3)$ group. $F^{a}_{\mu\nu}$ are the field strength tensors, A^{a}_{μ} being

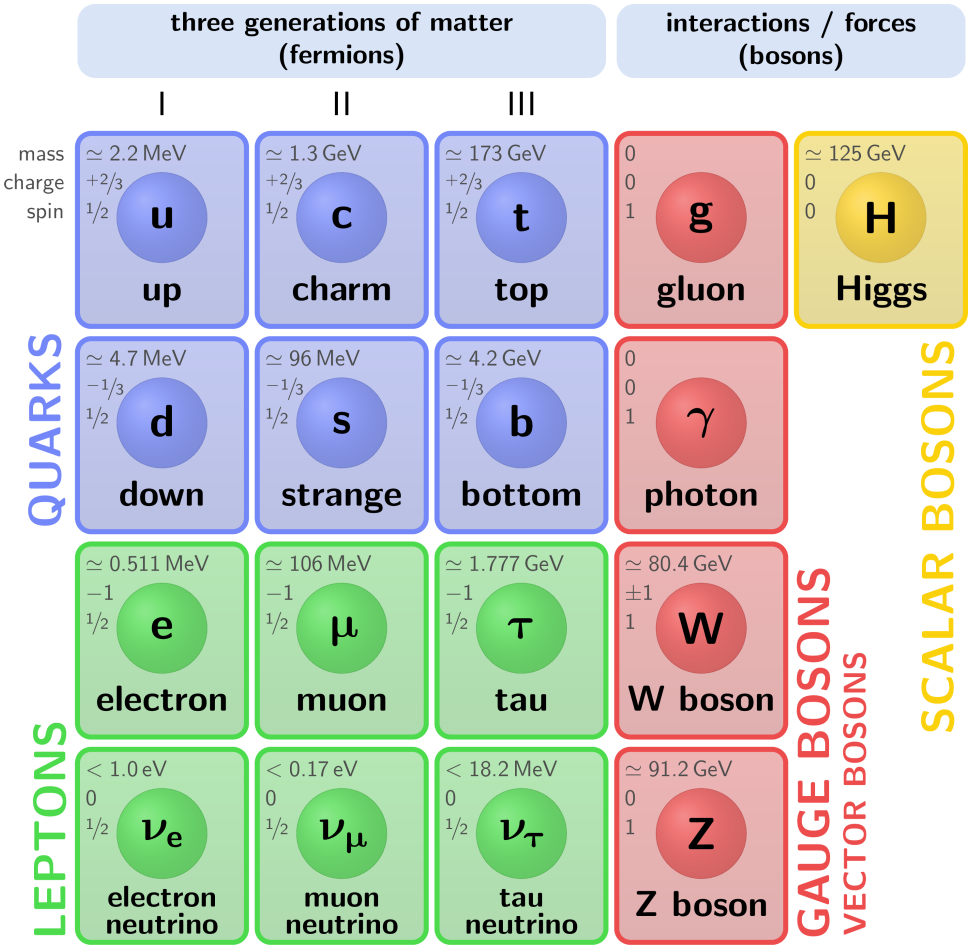

Figure 1.1: A schematic of the Standard Model showing its constituents [2].

the gluons. g is the strong coupling, T^a are the Gell-Mann matrices, and f^{abc} are the structure constants in the adjoint representation of the $SU(3)$ group. Unlike the QED Lagrangian, gauge transformations in QCD theory are non-Abelian. This allows for interesting phenomena to occur in particles and systems undergoing strong interactions that are not possible otherwise, if only electromagnetic interactions take place. For example, in QED, a photon cannot interact with itself. However, in Feynman diagrams representing QCD processes, gluon loops are also taken into account, because there exists a term in the field strength tensor that is quadratic in the fields (Eq.1.1). These contributions, combined with QED like contributions leads to a dependence of the strong coupling constant on the momentum of the exchanged gluon, which is strikingly different from the dependence of the QED coupling constant on the energy of the exchanged photon.

1.3 Running of the Coupling Constant

The QCD coupling constant is defined as

$$\alpha_S = \frac{g^2}{4\pi} \tag{1.2}$$

where the constant g can be referred from Eq.1.1. Its dependence on the energy of the exchanged gluon is shown in Fig. 1.2 [3]. It can be seen from Fig. 1.2 that α_S decreases as the momentum

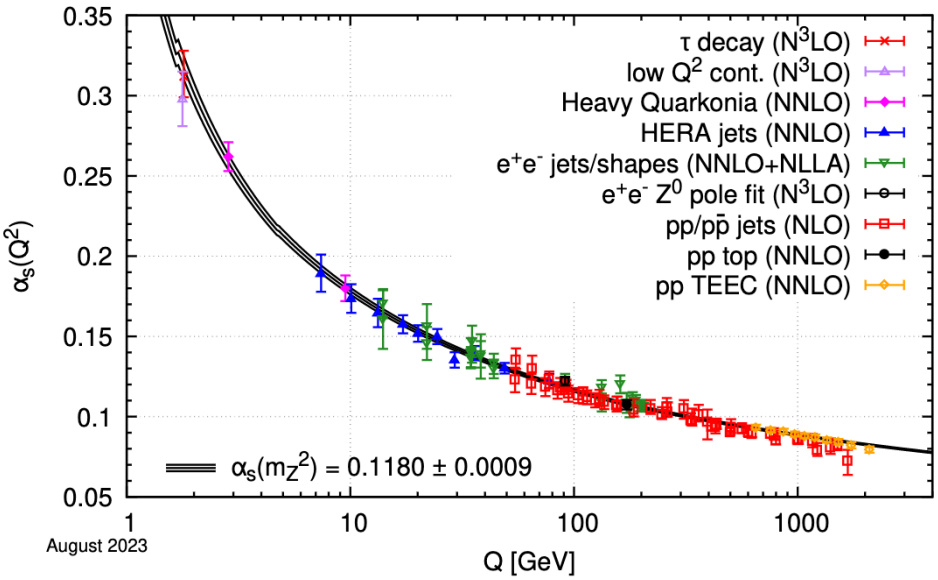

Figure 1.2: Different measurements of the strong coupling constant at the renormalization scale of the Z-boson mass [3].

of the exchanged gluon increases and vice versa. This energy dependence of the coupling constant is referred to as it's running. The theoretical formulation of running of α_S is given by [4]:

$$\alpha_S(\Lambda) = \frac{\alpha_S(\Lambda_0)}{1 + \left(\frac{33-2N_f}{6\pi}\right)\alpha_S(\Lambda_0)\ln(\frac{\Lambda}{\Lambda_0})} \tag{1.3}$$

where $\Lambda_0 = M_z c^2$, M_z being the Z-boson mass, and N_f is the number of quark flavors which can be produced in particle-antiparticle pairs at the given energy scale Λ, i.e., $m_q < \Lambda/2c^2$, m_q being the mass of the quark flavor.

1.3.1 Asymptotic Freedom

The decrease in the magnitude of the coupling constant with increasing energy of the exchanged gluon implies that in systems where the gluons exchanged between quarks and gluons (collectively referred to as partons) are of high momentum, there, the binding between the partons

would be weak, and the partons would be relatively free from the influence of each other in comparison to systems where exchanged gluons are of low energies. This phenomenon is referred to as *asymptotic freedom*. The momentum of the exchanged gluon is inversely proportional to the separation between partons, as the violation in conservation of momentum that happens due to the exchange of the off-shell bosons should be within the bounds set by the position-momentum uncertainty principle. Consequently, as the partons come closer together in space, the gluons being exchanged between them have higher momentum. By the running of the coupling constant (Fig. 1.2, Ref. [3; 4]), it is thus understood that the strong force between partons decreases as they are brought closer together. This will play an important role in the realm where the partons must be close together so that a large system of them could undergo thermalization.

1.3.2 Color Confinement

Quarks are fermions, and by Pauli's exclusion principle, it is known that a system of identical fermions must be in a state where the wavefunction is antisymmetric under the operation of particle exchange. Thus, baryons like $\Delta^{++}(uuu)$, cannot exist, given only the spin degree of freedom. Moreover, the total angular momentum deduced using the decays of this baryon suggests that all the three quarks are in the same spin state [5; 6]. Thus, there must be another degree of freedom, referred to as color, and associated to it is the quantum number called color charge. The space part, or the flavor part of the baryons could then be symmetric under constituent quark exchange and the color part can be antisymmetric. There are three color charges, denoted by r, g, b, which have nothing to do with colors in the visible light spectrum, but are quantum numbers alone. Till date, no free quarks, whose existence could be verified by the fractional electric charges that they carry, have been observed in nature. They are always found bound within hadrons, a fact which has been experimentally validated by deep inelastic scattering (DIS) experiments, whereby electrons with energies of the order of few GeV are fired at target nuclei in order to probe their internal structure [7]. This non-existence of free quarks in nature is explained by the *color confinement* hypothesis of the simple quark model, which states that those states of quarks that have an overall non-zero color charge cannot exist freely in nature. That is, quarks, which carry any one of the color charges, r, g, b cannot be isolated. They must be bound within hadrons, which do not have an overall net color charge. Color neutral combinations are the ones which have, either all three color states in an antisymmetric combination, as in the case of baryons (qqq), or in states that are composed of quarks in one color state and and an antiquark in the corresponding anticolor state, i.e., mesons $(q\bar{q})$. Although confinement on the existence of free quarks and gluons is a fundamental property of QCD, high temperature QCD predicts the formation of a plasma of quarks and gluons, which is studied using ultra-relativistic heavy-ion collisions.

1.4 The QCD Phase Diagram and QGP

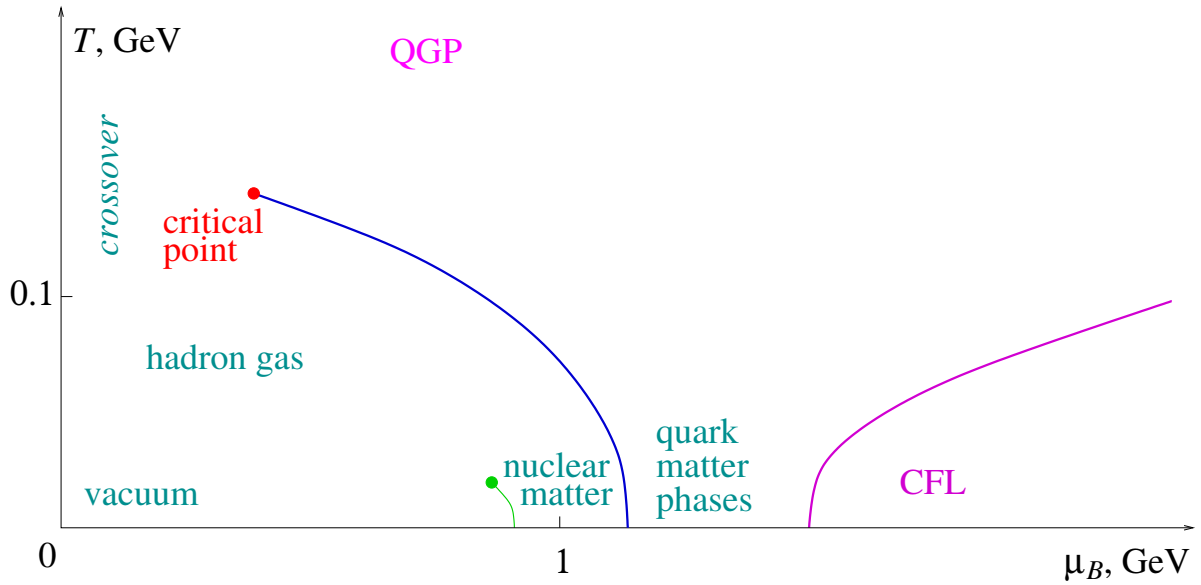

Figure 1.3: The QCD phase diagram, obtained from lattice QCD calculations. A crossover transition occurs to higher temperatures in the low μ_B regime. This is the region that is experimentally accessible to us using the current particle collider experiments. Blue line indicates a first order phase transition from baryonic matter (consists of hadron gas and nuclear matter) to QGP. The region enclosed by the magenta line consists of quarks in color flavor locked states, also referred to as color superconductors in analogy to QED superconductors [8].

With reference to Fig. 1.2, it can be seen that, as the energies of the exchanged gluons between the partons approaches values much lower than the renormalization scale (e.g., 1 GeV), the strong coupling constant starts to diverge. This implies that the QCD processes where partons have large separations, cannot be analyzed perturbatively, as the sum that corresponds to the matrix elements would diverge. Instead, non-perturbative approaches are required, and for that, there exists the theoretical framework of lattice QCD, which discretizes spacetime into a lattice, with lattice constant corresponding to the renormalization scale, and matrix amplitude calculations are then performed. From lattice calculations, the QCD phase diagram has been obtained, a schematic of which has been shown in Fig. 1.3 [8]. As pointed out at the end of Chapter 1.3.1, the transition from the limit of non-perturbative QCD to the realm of perturbative QCD, for systems with a large number of partons, a locally thermalized hydrodynamic state - the QGP [9; 10; 11] - is hypothesized to exist. Thermalization in QGP occurs due to strong interactions. Hence, its lifetime is expected to be of the order of 10^{-23} s. As a result, it cannot be observed directly and its existence and properties are instead inferred using indirect signatures like thermal photon production [12], quarkonia suppression [13], jet quenching [14], to name a few.

1.5 Ultra-Relativistic Heavy-ion Collisions

In the Large Hadron Collider (LHC), pp collisions are carried out at very high center of mass energies ($\sqrt{s}$ = 13.6 TeV). Although the number of partons that collide in such pp collisions are large, it is not large enough for local thermal equilibrium to be established. Hence, nuclei with large number of nucleons (e.g., Au in RHIC, Pb in LHC) are used in order to infer about the existence of QGP. Hence, Pb-Pb collisions at ultra-relativistic center of mass energies are carried out in the LHC, at $\sqrt{s_{\mathrm{NN}}}$ = 5.02 TeV. The various resultant distributions of the final state particles (e.g., in momenta, rapidity, etc.) are used to infer properties about the several stages that a heavy-ion collision is hypothesized to go through. An ultra-relativistic heavy-ion collision is analyzed experimentally by factoring it into several stages, as shown in Fig.1.4 [15].

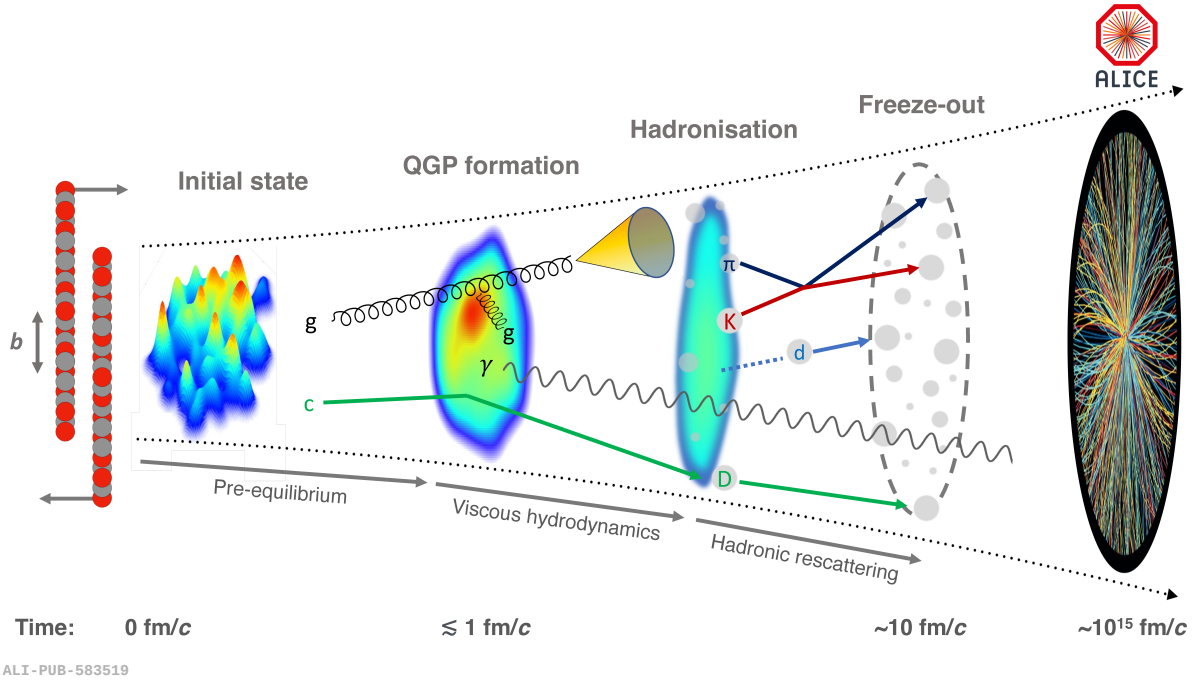

Figure 1.4: The several stages of evolution that an ultra-relativistic heavy ion collision is factored into [15].

Initially, the Pb nuclei - Lorentz contracted due to them having been boosted to energies much higher than their equivalent rest mass energy - collide. As a result of nucleon-nucleon collisions, a large amount of partons with high energy are deposited in the collision region in a pre-equilibrium state. They then undergo strong interactions to reach a state which is in local thermal equilibrium, and undergo collective expansion - referred to as the QGP phase. As expansion happens, the temperature of the QGP medium drops and partons start hadronizing at various regions within the medium (as and when the temperature drops below the pseudocritical temperature). The hadrons thus formed undergo collisions among themselves, largely inelastically. As the system evolves further and the inelastic collisions cease, the particle composition

of the system gets fixed and it is said to have reached chemical freezeout. The interactions thereafter are largely elastic collisions, which keep taking place until the mean free path of the hadrons is much larger than the system size. The system has then reached the kinetic freezeout. The momenta and the energy of particles are fixed by this point, and they stream freely to the detectors, where their properties are measured.

1.6 Anisotropic Flow and Symmetry Planes

Partons and energy within nuclei are not distributed uniformly throughout the nuclear region, and rather have a coarse structure due to being clumped within nucleons. This anisotropy of energy distribution is expected to impact the final state particle distribution as well, since QGP undergoes a viscous hydrodynamic expansion. More generally, if the response of the evolution of the system is linear to initial state geometry effects, then the geometrical symmetries of the anisotropy of initial state is expected to be reflected in the symmetries of anisotropy of the distribution of the final state hadrons in the momentum space. In order to quantify this anisotropy in the final state, the azimuthal distribution of final state hadrons in the transverse momentum plane is broken down into a Fourier sum [16; 17]:

$$f(\phi) = \frac{1}{2\pi}\left[1 + 2\left(\sum_{n>0} v_n \cos(n(\phi - \psi_n))\right)\right] \tag{1.4}$$

where ϕ denotes the angle in the azimuthal momentum plane. The coefficients v_n are referred to as the anisotropic flow coefficients, and ψ_n are called the symmetry plane angles of order n. Only the cosine terms are considered in the series because, in a given momentum range, the distribution of the particles should not be changed under the coordinate transformation $\phi \rightarrow -\phi$.

The anisotropic flow coefficients v_n quantify the overlap of the azimuthal distribution of the hadrons with different geometrical shapes. From the definition of anisotropic flow, we have for n^{th} order term, that it stays invariant under the transformation $\psi_n \rightarrow \psi_n + \frac{2\pi m}{n}$, where $m = 1, 2, 3, ..., n-1$. This property allows us to understand the geometrical implications of the terms in the Fourier sum. v_1 quantifies the overlap of the distribution with a directed line, oriented at an angle ψ_1 with respect to the p_x axis. A natural choice for the orientation of the azimuthal momentum coordinate system in an event is the reaction plane, which contains the beam axis and the impact parameter vector of the colliding nuclei. However, in the detectors attached to particle colliders, it is not possible to determine the reaction plane corresponding to an event. Hence, p_x axis is fixed by the setup of the detector system itself. So, v_2 denotes the overlap of the final state hadronic azimuthal distribution with an ellipse oriented at an angle ψ_2 with respect to the p_x axis. For $n \geq 3$, v_n denotes the overlap of the azimuthal distribution with a n-sided polygon, which is oriented at an angle ψ_n with respect to the p_x axis. From one event to another, as the orientation of the reaction plane changes, and the initial state fluctuates, the orientation of the symmetry planes also change. The method to compute the values of v_n and

ψ_n using multi-particle correlations in the final state, is as follows [18]:

$$v_{n_1}^{a_1} v_{n_2}^{a_2} \ldots v_{n_k}^{a_k} e^{i(a_1 n_1 \psi_{n_1} + a_2 n_2 \psi_{n_2} + \ldots + a_k n_k \psi_{n_k})} = \langle e^{i(n_1 \phi_1 + n_2 \phi_2 + \ldots + n_l \phi_l)} \rangle \tag{1.5}$$

where a_i are positive integers such that $\Sigma_i a_i = l$ and n_i are integers that could be both negative or positive. In the LHS of the above equation is a combination of the anisotropic flow terms, defined for a single event. The RHS denotes how the quantity on the LHS can be computed using multi-particle correlations, by averaging over all tracks that satisfy the cuts mentioned in Chapter 3.2. A choice of negative harmonics n_i, is possible because of the complex representation of the Fourier sum (Eq. 1.4), i.e.,

$$f(\phi) = \frac{1}{2\pi} \sum_{n \in \mathbb{Z}} v_n e^{i(n(\phi - \psi_n))} \tag{1.6}$$

where all the notation is the same as that used in Eq. 1.4. In order for Eq. 1.6 and Eq. 1.4 to be the same, we have that $\psi_n = \psi_{-n}$ and $v_n = v_{-n}$. Moreover, in Eq. 1.4, l particles are correlated such that a_i particles' azimuthal angles in the transverse momentum plane are multiplied with the harmonic order n_i and is summed, in order to fix the argument that goes into the exponential. Now, as the orientation of the reaction plane changes from event to event, no event averaged study of any particular ψ_n can be performed, as it will zero out across events.

So, typically, only the anisotropic flow coefficients have been analyzed to infer several properties of the collision system [19; 20]. However, if we want to find out the impact of the initial state geometry on the final state geometry, then, a great deal of information can be obtained if we could understand the orientation of ψ_n with respect to the reaction plane. However, due to trivial periodicity of the symmetry planes ($\psi_n \rightarrow \psi_n + \frac{2\pi m}{n}$ leaving the n^{th} flow term invariant), all the n symmetry planes of harmonic order n are equivalent. Hence, there lies an ambiguity in the choice of selecting which of them should be studied. In order to account for both these effects - trivial periodicity and random orientation of the reaction plane from one event to the other - symmetry plane correlations (SPCs) are the best quantities that can be studied. This can be achieved if in the argument in the LHS of Eq. 1.5, the coefficients a_i, n_i are chosen such that $\Sigma_{i=1}^{k} a_i n_i = 0$. Further elaboration on the appropriate choice of harmonic orders and the power to which they appear will be done in Chapter 2.

Previous investigations of SPCs were done in experiments [21; 22], with the aim of providing data that can be useful for development of event generation models using Bayesian estimation of parameters, as SPCs of different harmonic orders provide independent information about the final state geometry of an event. However, this investigation aims to use the physical inferences of SPCs in order to infer the geometrical properties of the initial state of the colliding system as per a transport model. An event shape [1] based analysis of SPCs is relevant majorly because SPCs deal entirely with the geometry of the event. The event shape is related again to the distribution of particles in the momentum space. Details of why the particular event shape

[1] What is referred to by 'event shape' is described at the beginning of Chapter 2.

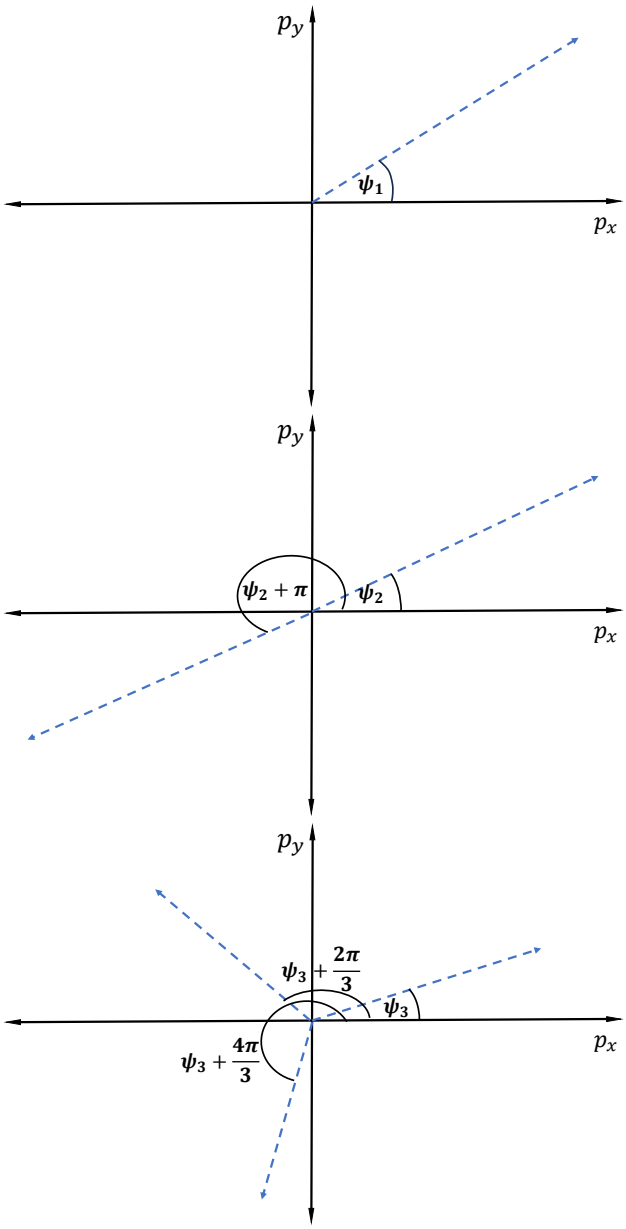

Figure 1.5: The physical meaning of different flow terms corresponding to harmonics $n = 1$ (top), $n = 2$ (middle), and $n = 3$ (bottom). The blue arrows indicate the orientation of the symmetry planes of respective orders. Symmetry in particle distribution arises because of the fact that picking a term corresponding to a particular harmonic, we have in Eq. 1.4 $f(\psi_n + \phi) = f(\psi_n - \phi)$ and the similarity with n-sided polynomial arises in addition to the fact that the transformation $\psi_n \rightarrow \psi_n + \frac{2\pi}{n}$ leaves the distribution $f(\phi)$ in Eq. 1.4 invariant. A depiction of the participat planes can be found in the Appendix 6.2.

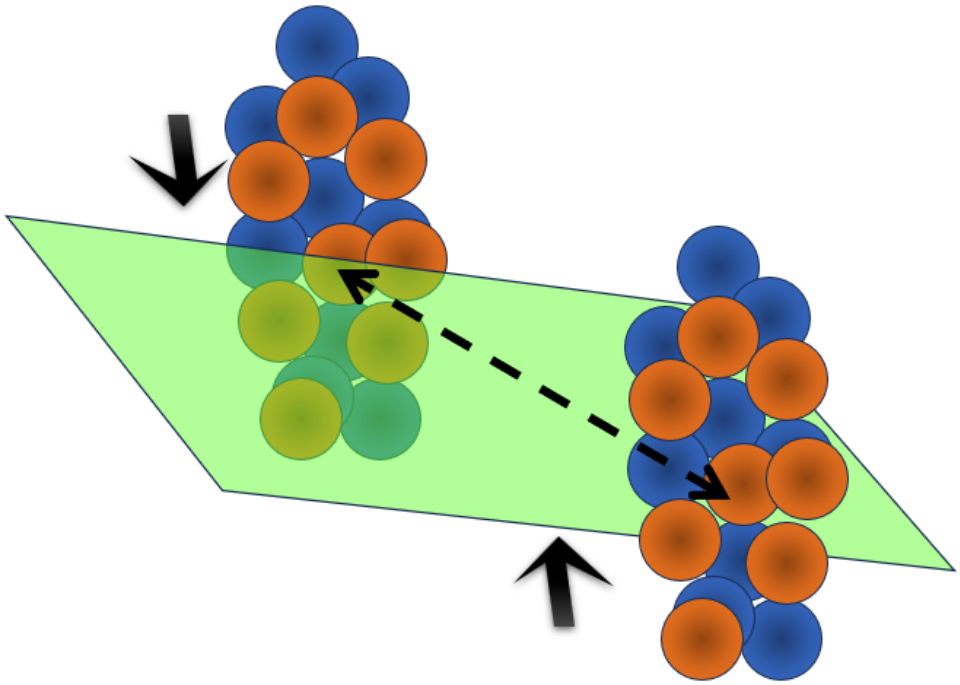

Figure 1.6: The figure above shows two nuclei moving into and out of the page with momenta as shown by solid black arrows - these are representative of the two oppositely moving collinear and parallel heavy-ion beams in the LHC. The black dotted line with arrows on both sides represents the impact parameter (the vector separating the centers of the two colliding nuclei). The transparent yellow-green plane represents the reaction plane - the plane spanned by the impact parameter and the beam axis. The centrality of a collision is the degree to which the centers of the two colliding nuclei overlap, which can be estimated using impact parameter in the heavy-ion collision event generator models directly, as has been pointed out in Table 3.1, or indirectly in experiments using the number of charged particles that finally emerge [23].

classifier, transverse spherocity has been used is given in Chapter 2.1.
The rest of the thesis goes on first to describe the mathematical formulation of the problem by defining the event shape classifier transverse spherocity, and symmetry plane and participant plane correlations in Chapter 2, followed by the methodology of event generation and event and track selection criteria in Chapter 3. The results are then presented in Chapter 4 and their inferences are elaborated in Chapter 5. Finally, a conclusive summary is given in Chapter 6.

Chapter 2

Problem Formulation

2.1 Transverse Spherocity

Before proceeding to describe the event-shape classifier transverse spherocity, it is important to define what is referred to by the event shape. The term event shape is used to describe the distribution in the azimuthal momentum space, of the final state particles which emerge in an event. Broadly an event is classified as having an isotropic or a jetty shape, as has been shown in Fig. 2.1. In order to perform this event-shape based study of SPCs, transverse spherocity (S_0) was used as the event shape classifier. It is defined as follows [24; 25]:

$$S_0 = \frac{\pi^2}{4} \min_{\hat{n}} \left[\left(\frac{\Sigma_i |\vec{p}_{T_i} \times \hat{n}|}{\Sigma_i |\vec{p}_{T_i}|} \right)^2 \right] \tag{2.1}$$

where $\vec{p}_{T_i}$ are the transverse momentum vectors and the summation index i runs over all charged hadronic tracks with $p_T > 0.15$ GeV/c and $|\eta| < 0.8$, and $\hat{n}$ is a parametric unit vector in the transverse plane, which would be used to minimize the quantity within the brackets. (The novice reader may refer to the Appendix (Chapter 6.2) for the definitions of the above mentioned quantities.) The constant $\frac{\pi^2}{4}$ is for the purpose of normalizing the value of S_0 to 1, in the case of a fully isotropic event shape. In the limit $S_0 \to 0$, the terms in the numerator would all tend to 0 as well, since they are all positive. So, $|\vec{p}_{T_i} \times \hat{n}| \to 0$ would mean that the transverse momenta vectors of the charged hadrons are all aligned along the direction given by $\hat{n}$. This is the case that the event is jetty. Conversely, in the case of an isotropic event, while some terms in the numerator are close to zero, others are far apart, and in the totally isotropic limit, $S_0 = 1$. these limits can be better visualized in the sketch Fig. 2.1 [26]. The S_0 for all real events will lie only between these two extremities considered. Previous studies have found out that S_0 is related to the elliptic flow [1] in an event [27]. Thus, other studies can be conducted to understand the effect of thermalization on the SPCs, but is not relevant directly to the work conducted towards this thesis. In this work, S_0 has been used only to classify events so that

[1] Refer to Fig. 1.5.

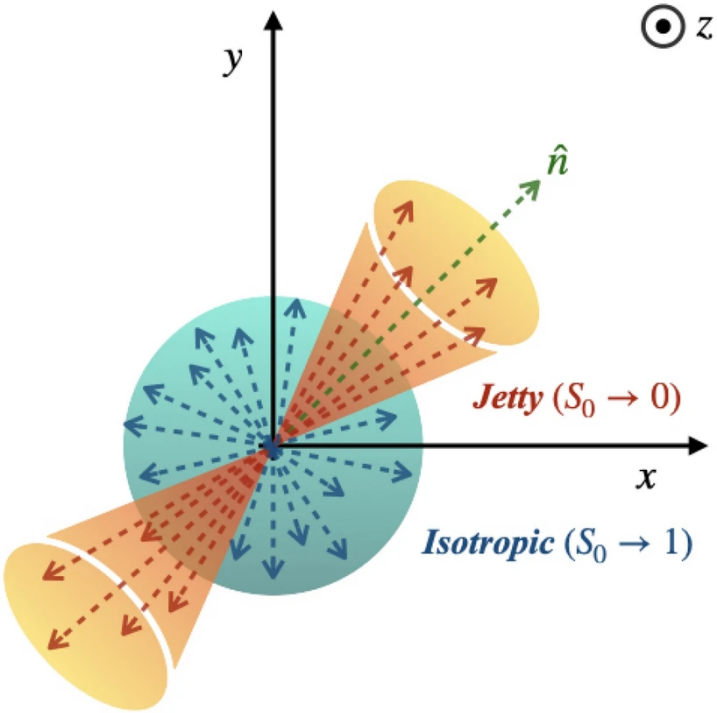

Figure 2.1: Depiction of the extreme limits of the jetty, or pencil-like and isotropic events and the values that S_0 would take in the corresponding events [26].

within a given centrality class [2], the behavior of SPCs can be studied and compared between those of pencil-like or isotropic events.

2.2 Symmetry Plane Correlations

The Gaussian Estimator (GE) of SPCs is defined as [21; 28]:

$$\begin{aligned}&\langle\cos\left(a_1 n_1\psi_{n_1} + a_2 n_2\psi_{n_2} + \ldots + a_k n_k\psi_{n_k}\right)\rangle_{GE}\\ &= \sqrt{\frac{\pi}{4}}\frac{\left\langle v_{n_1}^{a_1} v_{n_2}^{a_2}\ldots v_{n_k}^{a_k}\cos(a_1 n_1\psi_{n_1} + a_2 n_2\psi_{n_2} + \ldots + a_k n_k\psi_{n_k})\right\rangle}{\sqrt{\left\langle v_{n_1}^{2a_1} v_{n_2}^{2a_2}\ldots v_{n_k}^{2a_k}\right\rangle}}\end{aligned} \tag{2.2}$$

where averages in the numerator and the denominator in the RHS are calculated using events within a certain centrality and spherocity class, as described in Chapter 3.2. While evaluating the numerator and denominator in the RHS of the above equation, the appropriate choices of harmonics and their powers will be as per that pointed out in Eq. 1.5, keeping in mind that the correlations in both the numerator and denominator should remain invariant under the rotation of reaction plane and be free of the ambiguities of trivial periodicity of symmetry planes. The latter can be enforced by considering only linear combinations of $n\psi_n$ for all harmonic orders n. To elaborate why this is so, consider the least possible value that ψ_n can take in the particular

[2] Refer to Fig. 1.6 and Table 3.1.

event in the range $[0, 2\pi)$, and denote it by $\psi_n^{(0)}$. Then, the set of all possible values of the symmetry plane angles of harmonic order n are $\psi_n \in \{\psi_n^{(0)} + \frac{2\pi m}{n} \mid m = 0, 1, 2, ..., n-1\}$. This then leads to $n\psi_n \in \{n\psi_n^{(0)} + 2m\pi \mid m = 0, 1, 2, ..., n-1\}$. Clearly, when any linear combination of $n_i\psi_{n_i}$ are considered, with their respective coefficients being integers a_i, we have first, $a_i n_i \psi_{n_i} \in \{a_i n_i \psi_{n_i}^{(0)} + 2a_i m_i \pi \mid m_i = 0, 1, 2, ..., n_i - 1\}$, and consequently, $\Sigma_i\ a_i n_i \psi_{n_i} \in \left\{\left(\Sigma_i\ a_i n_i \psi_{n_i}^{(0)}\right) + 2\pi\ (\Sigma_i\ a_i m_i) \;\middle|\; m_i = 0, 1, 2, ..., n_i - 1\right\}$. The phase that remains behind is an integer multiple of 2π, and thus, calculating any trigonometric functions of this linear combination of angles would avoid the effect of trivial periodicity.

In order to enforce rotational invariance of SPCs, it is imperative to understand the role of reaction plane in the linear combination of the symmetry plane angles $\Sigma_i\ a_i n_i \psi_{n_i}$. By conservation of momentum, it is immediately understood that the system is symmetric under reflection of total transverse momenta in any infinitesimally small azimuthal angle range, about the reaction plane. So, the reaction plane happens to be a natural choice for the reference of symmetry plane angles. Thus, rotating our coordinates to account for this, we have that $\psi_n \to \psi_n - \Psi^*, \forall\ n \in \mathbb{N}$, where Ψ^* denotes the reaction plane angle in the laboratory coordinate system. Thus, the linear combination of angle that is free of trivial periodicity transforms as $\Sigma_i\ a_i n_i \psi_{n_i} \to \Sigma_i\ a_i n_i (\psi_{n_i} - \Psi^*) = \Sigma_i\ a_i n_i \psi_{n_i} - \Psi^*\ (\Sigma_i\ a_i n_i)$, as Ψ^* is a constant independent of the choice of the harmonic orders and their respective coefficients. Now, clearly, in order for $\Sigma_i\ a_i n_i \psi_{n_i}$ to be invariant under the rotation of the reaction plane, the second sum after the transformation shown in the last line should vanish. This can be enforced by making the choice $\Sigma_i\ a_i n_i = 0$.

When evaluating the SPCs, the coefficients a_i are always chosen to be positive. This is because, in both the numerator and the denominator, for every index i (Eq. 2.2), a_i happens to be the power to which the anisotropic flow coefficient v_{n_i} is raised. In order to understand the magnitude of these anisotropic flow coefficients, their definition, as given in Eq. 1.5 can be used. Considering only one, but any general harmonic n, we have $\langle v_n e^{in\psi_n} \rangle = \langle e^{in\phi} \rangle$. Now, it is clear that $|v_n| < 1\ \forall\ n \in \mathbb{Z}$. This is elaborated below:

$$v_n e^{in\psi_n} = \langle e^{in\phi} \rangle = \frac{\Sigma_{j=1}^{N_{\text{tracks}}}\ e^{in\phi_j}}{N_{\text{tracks}}}$$

where N_{tracks} is the total number of charged hadronic tracks which satisfy the cuts mentioned in Chapter 3.2. By the triangle inequality, it is clear that the complex number under consideration has a magnitude less than 1. By this, it can be understood that if $a_i < 0$ then the terms in the sum of the numerator and denominator could be very large, especially for events that have an isotropic distribution of final state particles. In order to avoid such divergences, all a_i must be positive. Hence, the condition $\Sigma_i\ a_i n_i = 0$ can be ensured by considering some of the harmonics to be negative, as such a choice neither affects ψ_n nor v_n, pointed out earlier, below Eq. 1.6.

To illustrate with an example, we can consider correlations between symmetry planes of harmonic orders $n = 2, 3, 5$. As seen above, since n can sometimes be taken to be negative, the

notation can be fixed as $|n_1| = 2,\ |n_2| = 3,\ |n_3| = 5$. To ensure rotational invariance we must have $a_1n_1 + a_2n_2 + a_3n_3 = 0$. This can be achieved with the choice $(a_1, a_2, a_3) = (1, 1, 1)$ and $(n_1, n_2, n_3) = (2, 3, -5)$. The argument that then goes into the combination of symmetry plane angles that will be correlated (Eq. 2.2) is $1 \times 2\psi_2 + 1 \times 3\psi_3 + 1 \times (-5\psi_{-5}) = 2\psi_2 + 3\psi_3 - 5\psi_5$. Now the corresponding SPC can be evaluated as follows:

$$\langle\cos(2\psi_2 + 3\psi_3 - 5\psi_5)\rangle_{GE} = \sqrt{\frac{\pi}{4}}\frac{\langle v_2v_3v_5\cos(2\psi_2 + 3\psi_3 - 5\psi_5)\rangle}{\sqrt{\langle v_2^2v_3^2v_5^2\rangle}}$$

It can be noted here that there are many other possible combinations of (a_1, a_2, a_3) and (n_1, n_2, n_3) consistent with the condition $\Sigma_i\ a_in_i = 0$ by scaling either of the set integers with a constant, i.e., $(a_1, a_2, a_3) \rightarrow (ra_1, ra_2, ra_3);\ r \in \mathbb{N}$, and $(n_1, n_2, n_3) \rightarrow (sn_1, sn_2, sn_3);\ s \in \mathbb{Z}$, leads to $\Sigma_i\ a_in_i \rightarrow \Sigma_i\ (ra_i)(sn_i) = rs\ \ (\Sigma_i\ a_in_i) = 0$, because to start with we have $\Sigma_i\ a_in_i = 0$. However, all these possible linear combinations of symmetry plane angles denote different multi-particle correlations and also provide independent information regarding the geometry of the final state [22]. Similarly, another possible combination of (a_1, a_2, a_3) and (n_1, n_2, n_3) under the constraint that $\Sigma_i\ a_in_i = 0$ is $(a_1, a_2, a_3) = (4, 1, 1)$ and $(n_1, n_2, n_3) = (2, -3, -5)$. This corresponds to the following SPC:

$$\begin{aligned}
&\langle\cos(4 \times 2\psi_2 + 1 \times -3\psi_{-3} + 1 \times -5\psi_{-5})\rangle_{GE} \\
&= \langle\cos(8\psi_2 - 3\psi_3 - 5\psi_5)\rangle_{GE} \\
&= \sqrt{\frac{\pi}{4}}\frac{\langle v_2^4v_3v_5\cos(8\psi_2 - 3\psi_3 - 5\psi_5)\rangle}{\sqrt{\langle v_2^8v_3^2v_5^2\rangle}}
\end{aligned} \tag{2.3}$$

Again, as will be shown in Chapter 5.4.3, this SPC has a very different centrality dependence in comparison to $\langle\cos(2\psi_2 + 3\psi_3 - 5\psi_5)\rangle_{GE}$, and hence provides independent information regarding final state geometry of the event. Finally, it must pointed out, how the calculation of the terms in the numerator and denominator happens for a single event, before taking an event average in the respective event shape and centrality class. To illustrate this, consider $\langle\cos(8\psi_2 - 3\psi_3 - 5\psi_5)\rangle_{GE}$. Corresponding to this SPC, we have the numerator term in Eq. 2.3 as:

$$v_2^4v_3v_5\cos(8\psi_2 - 3\psi_3 - 5\psi_5) = Re(v_2^4v_3v_5e^{i(8\psi_2 - 3\psi_3 - 5\psi_5)})$$

using Eq. 1.5, the above can be simplified as follows:

$$Re(v_2^4v_3v_5e^{i(8\psi_2 - 3\psi_3 - 5\psi_5)}) = Re\left(\left\langle e^{i(2\phi_1 + 2\phi_2 + 2\phi_3 + 2\phi_4 - 3\phi_5 - 5\phi_6)}\right\rangle\right)$$

Here, $(\phi_1, \phi_2, \phi_3, \phi_4, \phi_5, \phi_6)$ denotes the multiplet of azimuthal angles in the transverse momentum plane of six particles that satisfy the cuts mentioned in Chapter 3.2. The average on the RHS of the above equation is performed over all such possible multiplets $(\phi_1, \phi_2, \phi_3, \phi_4, \phi_5, \phi_6)$. For the denominator in Eq. 2.3, we have:

$$v_2^8v_3^2v_5^2 = \left[v_2^4v_3v_5e^{i(8\psi_2 - 3\psi_3 - 5\psi_5)}\right]\left[v_2^4v_3v_5e^{i(8\psi_2 - 3\psi_3 - 5\psi_5)}\right]^*$$

where, z^* denotes the operation of complex conjugation on the complex number z.

$$\therefore \;\; v_2^8 v_3^2 v_5^2 = |v_2^4 v_3 v_5 e^{i(8\psi_2 - 3\psi_3 - 5\psi_5)}|^2 = \left| \left\langle e^{i(2\phi_1 + 2\phi_2 + 2\phi_3 + 2\phi_4 - 3\phi_5 - 5\phi_6)} \right\rangle \right|^2$$

The average on the RHS of this equation is again calculated as pointed out earlier.

2.3 Participant Plane Correlations

By the virtue of the collective expansion of the QGP medium, the anisotropies in the distribution of energy in the initial state is expected to be carried over to the anisotropy of final state particles in the momentum space [16]. Thus, the geometrical analogue of the SPCs in the initial state, termed as the participant plane correlations (PPCs) will be defined using the eccentricities and the participant plane angles [29]. In order to construct GE of PPCs, defined in analogy with the GE of SPCs (Eq. 2.2), while being consistent with the definitions of eccentricities and participant planes [30; 31], the following definition of calculating them in a way similar to Eq. 1.5 is used:

$$\epsilon_{n_1}^{a_1} \epsilon_{n_2}^{a_2} \ldots \epsilon_{n_k}^{a_k} e^{i(a_1 n_1 \Phi_{n_1} + a_2 n_2 \Phi_{n_2} + \ldots + a_k n_k \Phi_{n_k})} = \frac{\left\langle r_1^{|n_1|} r_2^{|n_2|} \ldots r_l^{|n_l|} e^{i(n_1 \tilde{\phi}_1 + n_2 \tilde{\phi}_2 + \ldots + n_l \tilde{\phi}_l)} \right\rangle}{\left\langle r_1^{|n_1|} r_2^{|n_2|} \ldots r_l^{|n_l|} \right\rangle} \tag{2.4}$$

where ϵ_{n_i} are the eccentricities and Φ_{n_i} are the participant planes of the harmonic order n_i, r_j are the transverse positions of the participating nucleons with respect to the beam axis, $\tilde{\phi}_j$ are their azimuthal angles in the position space, transverse to the beam axis. Rest of the conditions for fixing a_i and n_i, on the left and right hand sides of Eq. 2.4 are the same as that used in Eq. 1.5. The quantity on the LHS of Eq. 2.4 is defined for a single event. The data of transverse positions is available in AMPT, which stores the initial nuclear configuration used for simulating an event. The RHS of Eq. 2.5 is an average over all the multiplets of wounded nucleons in the initial state. Using Eq. 2.4, the GE of PPCs is defined as follows:

$$\begin{aligned} &\left\langle \cos(a_1 n_1 \Phi_{n_1} + a_2 n_2 \Phi_{n_2} + \ldots + a_k n_k \Phi_{n_k}) \right\rangle_{GE} \\ &= \sqrt{\frac{\pi}{4}} \frac{\left\langle \epsilon_{n_1}^{a_1} \epsilon_{n_2}^{a_2} \ldots \epsilon_{n_k}^{a_k} \cos(a_1 n_1 \Phi_{n_1} + a_2 n_2 \Phi_{n_2} + \ldots + a_k n_k \Phi_{n_k}) \right\rangle}{\sqrt{\left\langle \epsilon_{n_1}^{2a_1} \epsilon_{n_2}^{2a_2} \ldots \epsilon_{n_k}^{2a_k} \right\rangle}} \end{aligned} \tag{2.5}$$

where the averages in the numerator and the denominator in the RHS of the above equation are computed over events in the centrality and spherocity classes, as defined in Chapter 3.2. As will be seen in Chapter 5.3, different linear combinations of participant plane angles, using which PPCs are calculated, also provide independent pieces of information regarding the initial state geometry, much in parallel with SPCs, as has been pointed out in Chapter 5.1.1 and Chapter 5.1.2. The calculation of the numerator and denominator terms event-by-event in Eq. 2.5 are the same as that described at the end of the last section, while keeping in mind, the definition in Eq. 2.4.

Chapter 3

Methodology

3.1 A Multi-Phase Transport Model

All the events are generated using A Multi-phase Transport model (AMPT) [32]. It is a transport model which simulates nucleus-nucleus collisions by dealing explicitly with the non-equilibrium dynamics. AMPT is used in the string melting mode. It factors the nucleus-nucleus collisions into four stages. Firstly, the nuclei are initialized using the HIJING framework [33]. The initialization happens as per the Glauber model [34]. The wounded nucleons are then fragmented into partons and the consequent partonic interactions are modeled using the Zhang's Parton Cascade (ZPC) framework [35]. When the partons have stopped colliding with other partons, they are then hadronized by coalescing with other partons which are close by in the phase space [36]. The rescatterings among the resultant hadrons are then modeled using A Relativistic Transport (ART) framework [37]. This entire scheme is illustrated in Fig. 3.1.

The center of mass energy of the colliding $^{208}_{82}$Pb nuclei was set to $\sqrt{s_{\rm NN}}$ = 5020 GeV. The hadron cascade time was set to 30 fm/c. The parameters 'a' and 'b' in the Lund symmetric splitting function [38] were set to, a = 0.30 and b = 0.15. The parton screening mass [35] was set to 1.2408 fm^{-1}. Flags for shadowing, initial and final state radiation, and for random orientation of the reaction plane were kept 'on'. Flags for K^S_0 weak decays, ϕ and π^0 decays at the end of hadron cascade, and for perturbative deuteron calculations were kept 'off'. In total, 107,000 events of Pb-Pb collisions in minimum bias were generated for the purpose of event-shape differentiated study of SPCs.

3.2 Event and Track Selection

In order to evaluate the SPCs (Chapter 2.2), only those events with at least five charged hadronic tracks with $p_T > 0.15$ GeV/c and $|\eta| < 0.8$ are considered. This criteria is necessary to have a well-defined S_0 [24]. Simultaneously, this criteria also feasibly fixes the meaningfulness of the multi-particle correlations that are to be performed as pointed in Eq. 1.5, i.e., there should

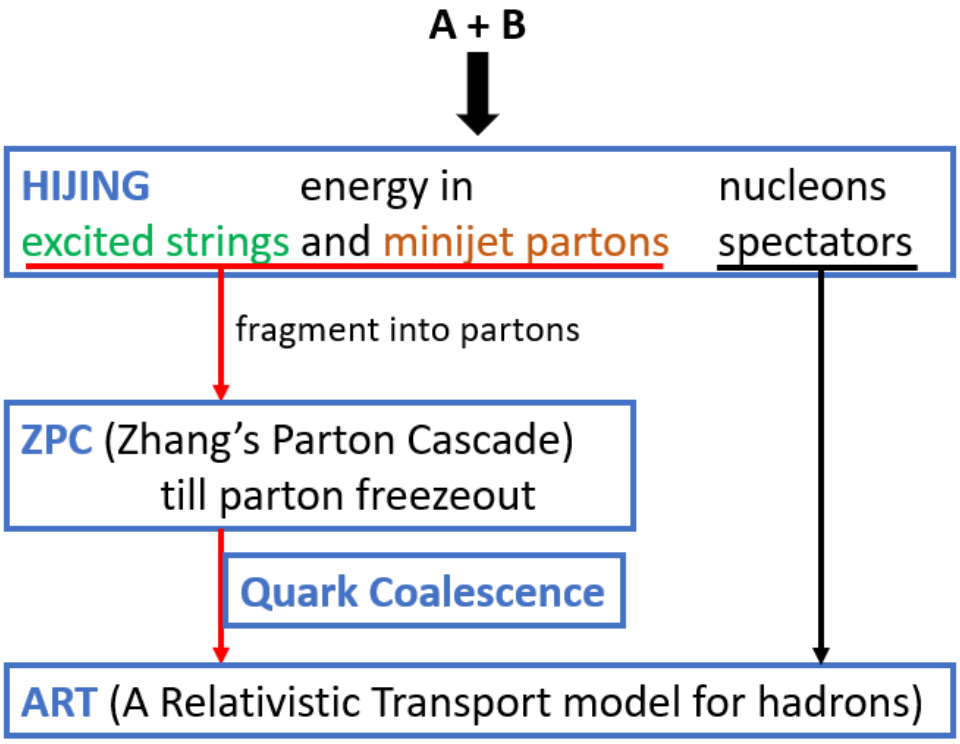

Figure 3.1: Flowchart of the stages that a heavy ion collision undergoes, as per the AMPT model in the string melting mode [32].

be at least as many tracks in an event as are being correlated. Furthermore only those tracks with transverse momenta $0.2 < p_T < 5.0$ GeV/c and pseudorapidity $|\eta| < 0.8$ have been used for the multi-particle correlations in Eq. 1.5. These cuts are in order to be conduct an analysis consistent with experiment [21]. The centrality classification (shown in Table 3.1) for this investigation of SPCs has been performed as per the Glauber Monte Carlo scheme [39]. In each centrality class, the events have a distribution of S_0, and thus 20% events with the highest S_0 are classified as high-S_0, or isotropic, and 20% of the events with the least S_0 are classified as low S_0, or pencil-like. The numerical values of all the cuts described in this section are shown in Table 3.1.

Peripheral events (with centrality percentile larger than 60%) have not been considered for two major reasons. Firstly, the analysis of SPCs have not been performed on them because they yield very few tracks that satisfy all the cuts listed above in this section. As a consequence, the correlations in Eq. 1.5 become ill defined. That however, is only a problem in the case of ultra-peripheral collisions. The second and the more pertinent reason for which SPCs of peripheral events were not studied is because, the GE of the SPCs have been investigated in this study, which bases its formulation of SPCs on the fundamental assumption that the number of tracks in an event is always large enough for the central limit theorem to be applicable on the distribution of flow vectors. In other words, the real and imaginary parts of $v_n e^{in\psi_n}$ should

Centrality [%]	b (fm)	Low-S_0	High-S_0
0-5	0-3.49	0-0.897	0.958-1
5-10	3.49-4.93	0-0.859	0.942-1
10-20	4.93-6.98	0-0.810	0.912-1
20-30	6.98-8.55	0-0.764	0.881-1
30-40	8.55-9.87	0-0.734	0.869-1
40-50	9.87-11	0-0.719	0.869-1
50-60	11-12.1	0-0.718	0.876-1

Table 3.1: Centrality and S_0 classification of Pb-Pb collisions generated at $\sqrt{s_{\mathrm{NN}}}$ = 5.02 TeV using AMPT. 'b' denotes the impact parameter. Centrality class is represented by its equivalent percentile range.

follow a double-Gaussian distribution in the Argand plane [1].

[1]The plane representing the complex number $z = x + iy$ as the coordinate (x, y) is referred to as the Argand plane.

Chapter 4

Results

In this section, the results obtained after evaluating the SPCs and PPCs, computed using the events from their respective event classes as described in Chapter 3.2 are shown and these results are then discussed in detail in Chapter 5. The classification of correlators as "int-S_0" (acronym for integrated-S_0) refers to the SPCs and PPCs being evaluated using all the events within a centrality class, and have consistently been represented by the black colored lines in all the plots included this chapter. Similarly, the classification of correlators as "high-S_0" and "low-S_0" refer to SPCs and PPCs that are evaluated using only those events within the centrality class for which the values of S_0 is in the range specified in the columns titled "high-S_0" and "low-S_0" in Table 3.1 respectively. The SPCs and PPCs evaluated using high-S_0 and low-S_0 events have respectively been shown using blue and red lines or markers in all the plots presented in this chapter.

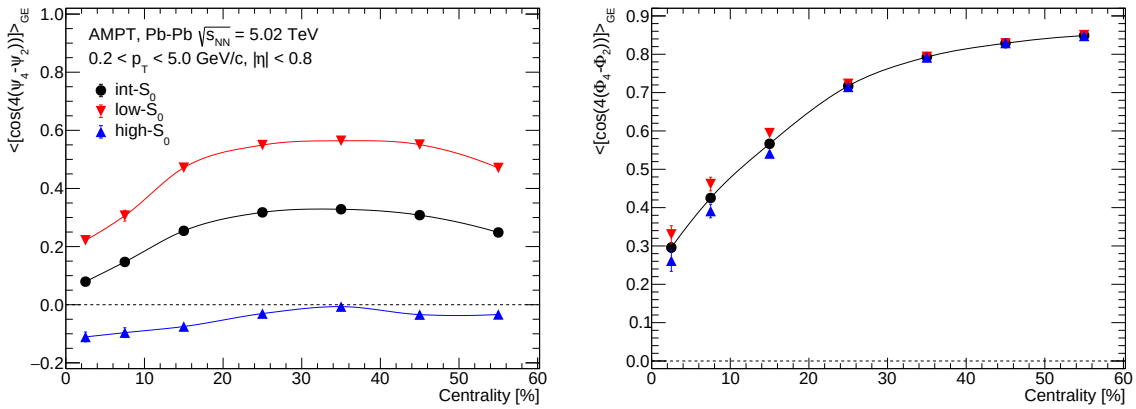

Figure 4.1: The centrality dependence of the SPC $\langle\cos(4(\psi_4 - \psi_2))\rangle_{GE}$ (left) and PPC $\langle\cos(4(\Phi_4 - \Phi_2))\rangle_{GE}$ (right), when calculated using events in different S_0 classes within each centrality class.

In Fig. 4.1, Fig. 4.2, and Fig. 4.3, the SPCs which are evaluated using events of all S_0 values, all increase in the most central classes to reach a maximum in the mid-central classes

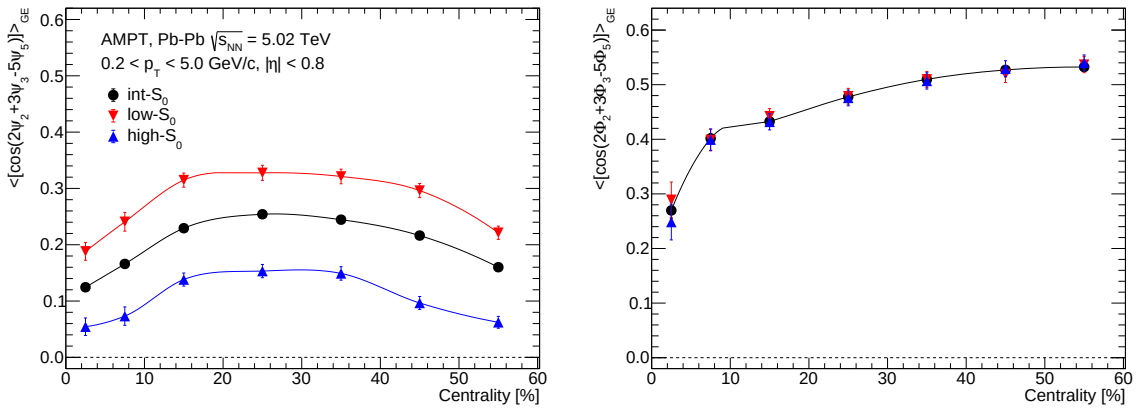

Figure 4.2: The centrality dependence of the SPC $\langle\cos(2\psi_2 + 3\psi_3 - 5\psi_5)\rangle_{GE}$ (left) and PPC $\langle\cos(2\Phi_2 + 3\Phi_3 - 5\Phi_5)\rangle_{GE}$ (right), when calculated using events in different S_0 classes within each centrality class.

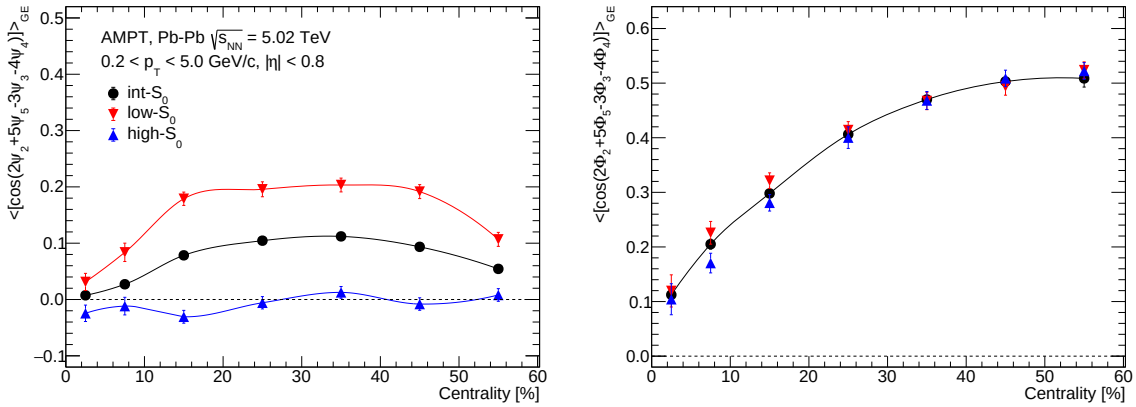

Figure 4.3: The centrality dependence of the SPC $\langle\cos(2\psi_2 + 5\psi_5 - 3\psi_3 - 4\psi_4)\rangle_{GE}$ (left) and PPC $\langle\cos(2\Phi_2 + 5\Phi_5 - 3\Phi_3 - 4\Phi_4)\rangle_{GE}$ (right), when calculated using events in different S_0 classes within each centrality class.

and then decrease again towards the peripheral event classes. It can also be seen that the values of the SPCs that are calculated using the low-S_0 events in Fig. 4.1, Fig. 4.2, and Fig. 4.3, are all consistently higher than those computed using both, the isotropic, or the S_0-integrated events. For $\langle\cos(2\psi_2 + 3\psi_3 - 5\psi_5)\rangle_{GE}$ the SPC evaluated using high-S_0 events is smaller in magnitude but has the same centrality dependence as the SPC evaluated using events of all shapes (Fig. 4.2). For $\langle\cos(4(\psi_4 - \psi_2))\rangle_{GE}$, the SPC obtained using high-S_0 events alone, is negative across all centrality classes (Fig. 4.1), and has a magnitude less than or equal to the corresponding SPC evaluated using events of all shapes. In the case of $\langle\cos(2\psi_2 + 5\psi_5 - 3\psi_3 - 4\psi_4)\rangle_{GE}$, the SPC evaluated using only high-S_0 events has values that oscillate about zero, as we move from the most central to the peripheral event classes.

The SPCs shown in Fig. 4.4 and Fig. 4.5, which are evaluated using either events of all

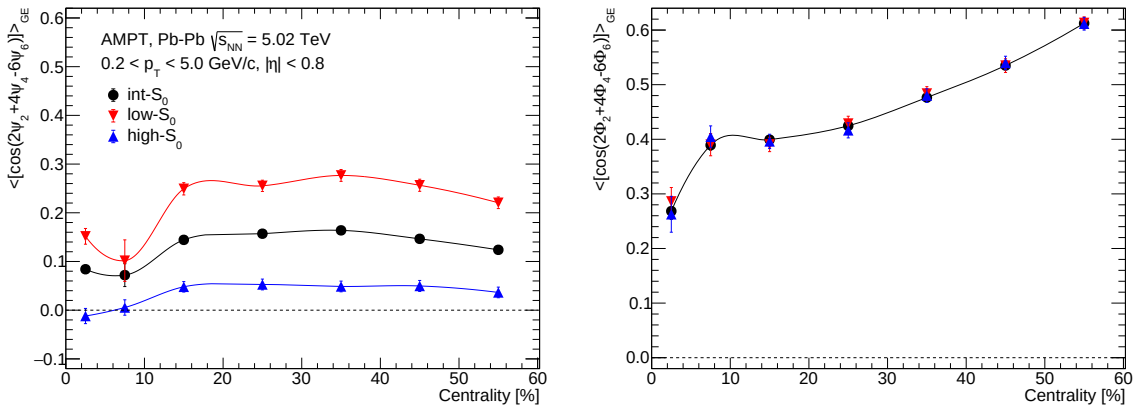

Figure 4.4: The centrality dependence of the SPC $\langle\cos(2\psi_2 + 4\psi_4 - 6\psi_6)\rangle_{GE}$ (left) and PPC $\langle\cos(2\Phi_2 + 4\Phi_4 - 6\Phi_6)\rangle_{GE}$ (right), when calculated using events in different S_0 classes within each centrality class.

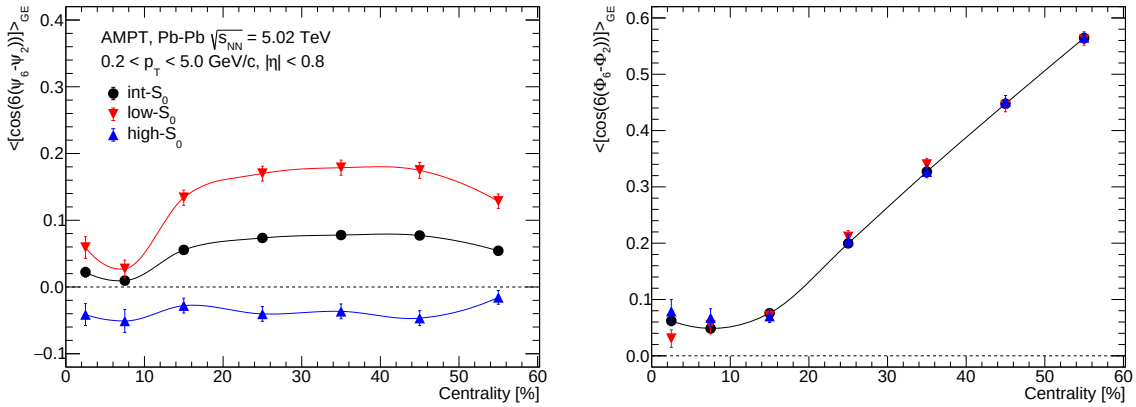

Figure 4.5: The centrality dependence of the SPC $\langle\cos(6(\psi_6 - \psi_2))\rangle_{GE}$ (left) and PPC $\langle\cos(6(\Phi_6 - \Phi_2))\rangle_{GE}$ (right), when calculated using events in different S_0 classes within each centrality class.

shapes or using only the low-S_0 events, show a decrease as we move from the 0-5% to the 5-10% most central class. They then increase and reach a maximum at the mid-central classes and then decrease again towards the peripheral event classes. The SPCs evaluated using only the high-S_0 events in Fig. 4.4 and Fig. 4.5 keep fluctuating about zero as we move from the most central to the mid-central event classes.

The SPC $\langle\cos(6(\psi_6 - \psi_3))\rangle_{GE}$ (Fig. 4.6) increases from the 0-5% centrality, reaches a peak in the 10-20% centrality class and keeps decreasing as one moves towards the more peripheral event classes. The SPC in Fig. 4.6 which is calculated using high-S_0 events has the same values as that of the SPC calculated using events of all shapes, whereas the SPC evaluated using low-S_0 events has values similar to that of int-S_0 SPC, except for the 20-30% most central class of events. The SPC $\langle\cos(2\psi_2 + 4\psi_4 - 6\psi_3)\rangle_{GE}$ shown in Fig. 4.7 is negative for all except the

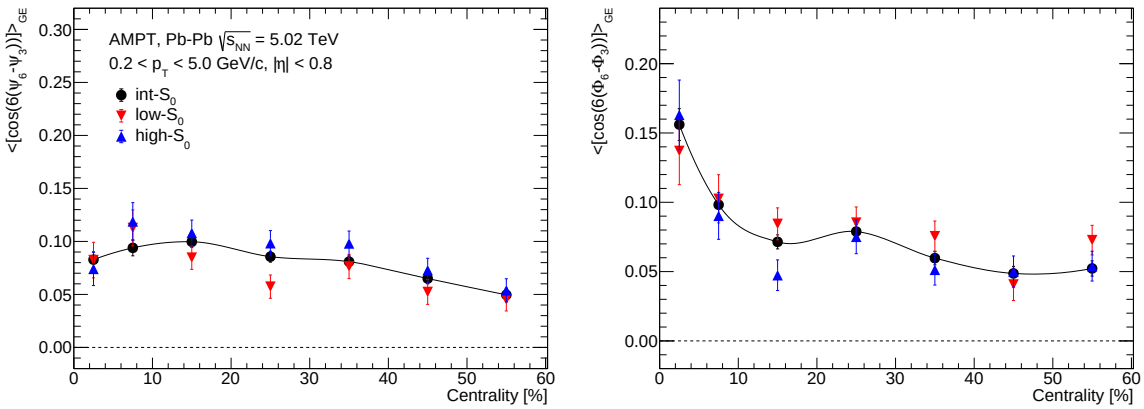

Figure 4.6: The centrality dependence of the SPC $\langle\cos(6(\psi_6 - \psi_3))\rangle_{GE}$ (left) and PPC $\langle\cos(6(\Phi_6 - \Phi_3))\rangle_{GE}$ (right), when calculated using events in different S_0 classes within each centrality class.

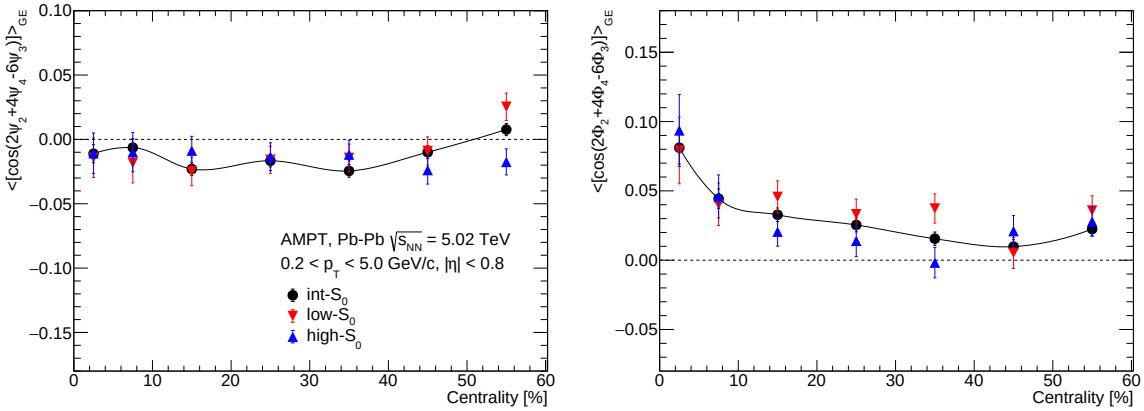

Figure 4.7: The centrality dependence of the SPC $\langle\cos(2\psi_2 + 4\psi_4 - 6\psi_3)\rangle_{GE}$ (left) and PPC $\langle\cos(2\Phi_2 + 4\Phi_4 - 6\Phi_3)\rangle_{GE}$ (right), when calculated using events in different S_0 classes within each centrality class.

most peripheral class of events, and the SPCs evaluated in the low and high S_0 event classes have same values within statistical errors as of the SPC evaluated using events of all shapes.

Shown in Figs. 4.8 and 4.9 are the SPCs $\langle\cos(6(\psi_3-\psi_2))\rangle_{GE}$ and $\langle\cos(8\psi_2-3\psi_3-5\psi_5)\rangle_{GE}$ respectively, both of which fluctuate about zero as we move from the most central to the peripheral event classes. The values of these SPCs that are evaluated correspondingly using either the low-S_0 or high-S_0 events alone are the same as the SPC evaluated using events of all shapes, the only exception being of the latter in 10-20% most central event class.

Finally it must be pointed out, that, all the PPCs shown in Figs. 4.1 to 4.9, have the same values with errors, across different event shape classes. While some of them have strikingly similar behavior with that of their corresponding SPCs, some display a different centrality dependence. In the next chapter, it will be shown whether there is a link between the SPCs

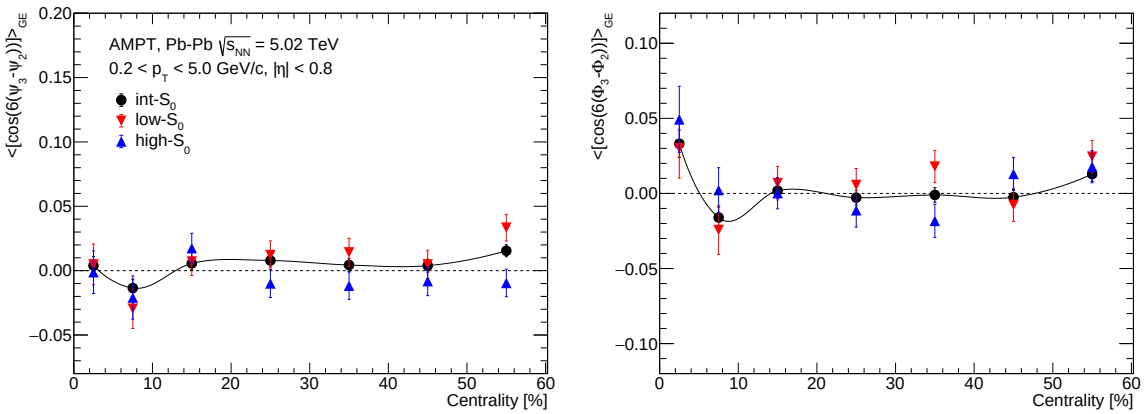

Figure 4.8: The centrality dependence of the SPC $\langle\cos(6(\psi_3 - \psi_2))\rangle_{GE}$ (left) and PPC $\langle\cos(6(\Phi_3 - \Phi_2))\rangle_{GE}$ (right), when calculated using events in different S_0 classes within each centrality class.

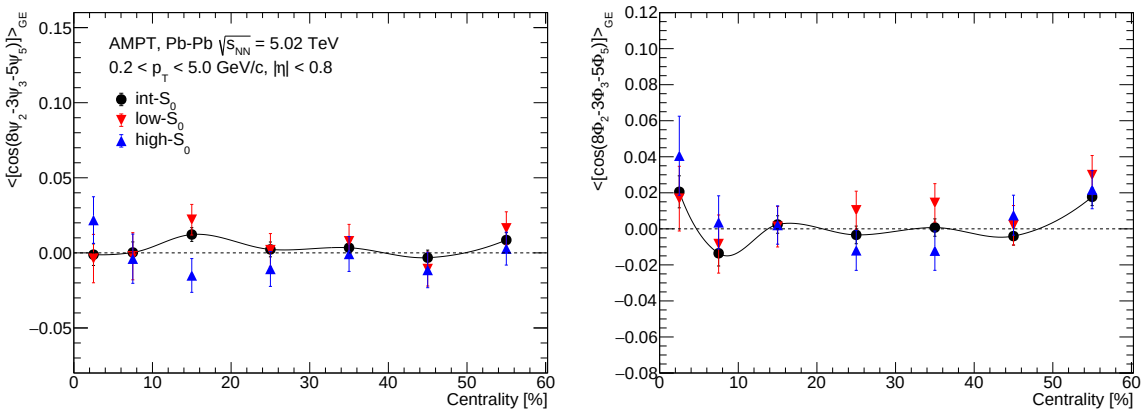

Figure 4.9: The centrality dependence of the SPC $\langle\cos(8\psi_2 - 3\psi_3 - 5\psi_5)\rangle_{GE}$ (left) and PPC $\langle\cos(8\Phi_2 - 3\Phi_3 - 5\Phi_5)\rangle_{GE}$ (right), when calculated using events in different S_0 classes within each centrality class.

and PPCs and if the relationship is linear. But before that, other interpretations of these results pertaining to the geometry of the collision system will be discussed.

Chapter 5

Discussion

In general, the SPCs give a measure of how close a linear combination of the symmetry planes of different harmonic orders are to zero, and thus correlated. When a combination of symmetry plane angles is considered, it is trivially expected that when only the low-S_0 events are taken into account for their evaluation, the SPCs will be larger than when considering event averages using events of all shapes. This is because, the numerator terms in Eq. 2.2 from low-S_0 events have contributions, whose real parts are closer to 1. This can be seen as follows:

$$\begin{aligned}\lim_{S_0\to 1} v_{n_1}^{a_1} v_{n_2}^{a_2} \ldots v_{n_k}^{a_k} e^{i(a_1 n_1 \psi_{n_1} + a_2 n_2 \psi_{n_2} + \ldots + a_k n_k \psi_{n_k})} &= \lim_{\phi_i \to \phi_0} \left\langle e^{i(n_1\phi_1 + n_2\phi_2 + \ldots + n_l\phi_l)} \right\rangle \\ &= \left\langle e^{i(n_1+n_2+\ldots+n_l)\phi_0} \right\rangle \\ &= \langle 1 \rangle \qquad \left[\because \ \Sigma_{i=1}^{l} n_i = 0\right] \\ &= 1\end{aligned}$$

The above represents the extreme limit that the event is jetty, and all the particles emerge collimated along the azimuthal direction characterized by the angle ϕ_0 with respect to the coordinate axes. This however, is illustrative of the fact that, within a given centrality class, the events which are classified as low-S_0 are going to have a contribution that is larger in the numerator of Eq. 2.2. Thus, when only the low-S_0 events within a centrality class are used for evaluating the SPCs, they should be larger, and more positive, in comparison to the SPCs which are evaluated using events of all shapes. For the case of isotropic events, the limit described above does not exist, as there is no particular correlation between the azimuthal angles of the tracks. Their contribution to the numerator in Eq. 2.2 can be positive, negative or zero, depending upon the azimuthal angular distribution of particles in that specific event.

All this, conclusively points towards the fact that the magnitude of the SPCs that are evaluated using low-S_0 events should be larger than those which are computed using either only high-S_0 events, or events of all shapes. If a deviation from this order happens, then it is to be understood that the event-by-event (EbE) fluctuations of azimuthal angles of emergent particles have a significant role in determining the value of that particular SPC.

Further, when the most central events are considered, the final particle distribution is expected

to be more isotropic than in the events of other centrality classes, as the multiplicity (number of final state particles) is very high, and the collision is head-on, leading to a high degree of isotropy starting right from the initial state. Such an isotropy will cause the SPCs to take on lesser values in the most central event class than in the mid-central event class. However, towards the peripheral event classes, the multiplicity decreases and the event then starts to take on different shapes, which would be determined by the initial condition and the evolution of the collision system. Hence, we cannot conclude about whether a SPC will be larger in the peripheral event classes in comparison to the most or the mid-central event classes.
If a SPC has a higher value in the most central event classes when compared to other centrality classes, then it can again be inferred that the SPC is sensitive to EbE geometrical fluctuation. Finally, if a SPC fluctuates about zero within errors across all centrality classes, and its values when computed using events of different S_0 classes are the same, then it can be concluded that the symmetry plane angles are decorrelated in the sense of the particular linear combination being considered.

5.1 Geometrical Interpretation of SPCs

5.1.1 SPCs of Symmetry Planes ψ_{2n} and ψ_2

Consider a system where for an integer n, the anisotropy of order $2n$ is dominant. Quantitatively, this will be characterized by a higher value of v_{2n} in comparison to $v_{m\neq 2n}$. If we have at least $4n$ particles ($2n$ to define the vertices of a $2n$-sided polygon, and $2n$ further particles to lie along the midpoints of the lines joining these $2n$ vertices), then the geometry of the final state can be well approximated by a $2n$-sided regular polygon. Thus, if at least $4n$ hadrons are present in the final state of events belonging to a centrality class, we can conclude v_{2n} in that centrality class to be indicative of the fact that the particle distribution can be described by a $2n$-sided regular polygon. An illustrative diagram of this discussion is presented in Fig. 5.1 for the case of $n = 2$ and $n = 3$. For the purposes of this thesis, the highest value that n takes is 6. Hence, for the geometrical arguments in the rest of this section to be applicable, there must be at least 24 particles present in the final state which satisfy the constraints mentioned in Chapter 3.2. This is practically met in the case of Pb-Pb collisions at $\sqrt{s_{\mathrm{NN}}} = 5.02$ TeV [40]. (In the AMPT generated event dataset that was used for this analysis, the minimum number of particles satisfying the cuts in Chapter 3.2, that were present in all considered centrality classes, is 39.)
Now, given a $2n$-sided regular polygon, we know that there exist n diameters (diagonals joining a pair of vertices farthest from each other), which in turn act as n different ψ_2. These can be visualized in Fig. 5.1 as either the n distinct double-sided solid arrows, or the n distinct end-to-end dashed lines, for the two cases shown. This being the case, we expect that there will typically be a strong correlation between symmetry planes of orders $2n$ and 2, i.e., among ψ_{2n} and ψ_2. The simplest correlator that can be defined using ψ_{2n} and ψ_2, that is one involving the

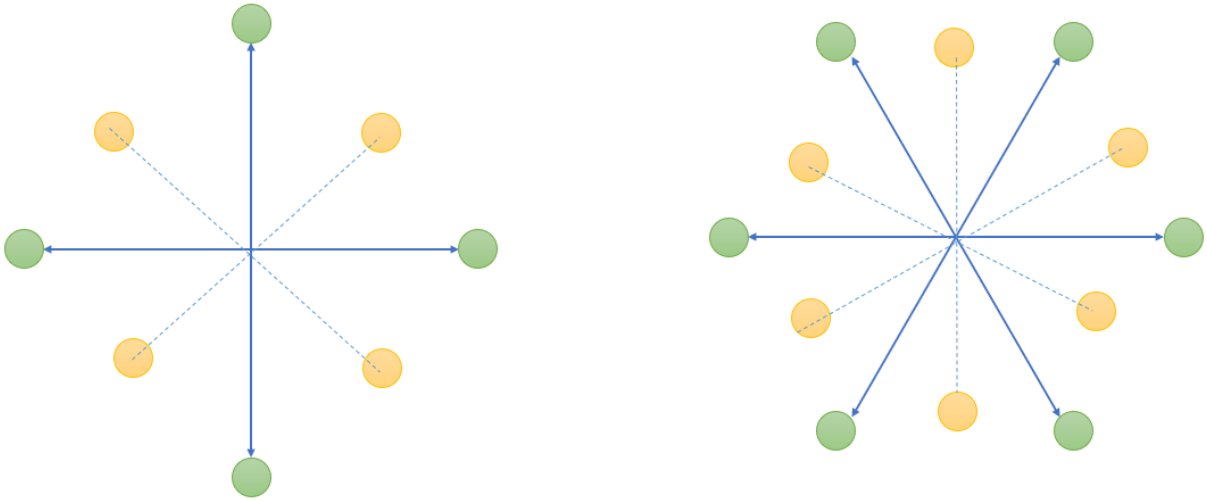

Figure 5.1: Figure showing the anisotropy of orders $2n$ being a regular polygon of $2n$ sides, requiring at least $4n$ particles, for the case of $n = 2$ (left) and $n = 3$ (right). The solid arrows and dashed lines represent azimuthal directions along which particle number density must be respectively same in the transverse momentum plane. The different colors are to point out that the number density in regions of one color need to be the same, but not otherwise. These inferences have solely been drawn from trivial periodicity of symmetry planes along with the fact that for a symmetry plane ψ_n, the distribution of particles is such that $f(\psi_n+\phi) = f(\psi_n-\phi)$, where $f(\phi)$ can be referred to from Eq. 1.4.

least number of particle correlations, is $\langle\cos(2n(\psi_{2n} - \psi_2))\rangle_{GE}$. This correlator having a high magnitude in a centrality class where the condition described in the last paragraph are met, in comparison to a centrality class where EbE fluctuations are known to dominate, would thus be an indicator of $2n$-ordered anisotropy being present.

5.1.2 SPCs of Symmetry Planes ψ_{2n} and ψ_n

Consider again a general integer n, and that the magnitude of v_{2n} is high for a certain centrality class where the conditions stated at the beginning of Chapter 5.1.1 are met. We also have the geometrical fact that in a $2n$-sided regular polygon, there are 2 distinct n-sided regular polygons as well. Hence, the presence of anisotropy of harmonic order $2n$ will also mean that there is a strong correlation between symmetry planes of order n and $2n$, i.e., among ψ_{2n} and ψ_n. The simplest correlator that can be constructed using these symmetry planes is $\langle\cos(2n(\psi_{2n} - \psi_n))\rangle_{GE}$. Hence, given a dominant anisotropy of order $2n$, we have that all symmetry planes which are obtained by halving $2n$ will be correlated.

The above property of the SPCs ensures that we can very clearly find out which order of anisotropy is most sensitive to EbE fluctuation of the final state particle azimuthal distribution. In addition, using the reverse argument stated at the end of the last paragraph, we could also

rule out the presence of higher order anisotropies in a system using SPCs of lower harmonics. As an example, if either $\langle\cos(2n(\psi_{2n}-\psi_2))\rangle_{GE}$ or $\langle\cos(2n(\psi_{2n}-\psi_n))\rangle_{GE}$ are zero across all centrality classes, then we could directly rule out the significance of the anisotropy of order $4n$.

5.2 Role of the Coefficients a_i in SPCs

The coefficients a_i that appear in a SPC as $\langle\cos(a_1n_1\psi_{n_1}+a_2n_2\psi_{n_2}+...+a_kn_k\psi_{n_k})\rangle_{GE}$, are not just playing the role of making $\Sigma_i\ a_in_i=0$ for rotational invariance. In fact, each a_i is also assigning the 'importance' that the anisotropy of order n_i has in the corresponding SPC. This is understood by observing that the index of v_{n_i} is a_i in the numerator terms of Eq. 2.2. So, if n_i is the dominant order of anisotropy, then each term in the numerator will be larger when the corresponding a_i will be larger. Consider for example, the case illustrated in Chapter 2.2 involving the harmonics $n=2,3,5$. When $a_1=a_2=a_3=1$, then the coefficient that appear in the numerator terms of the SPC are $v_2v_3v_5$. However, for the case where $a_1=4$ and $a_2=a_3=1$, the corresponding weight factor is $v_2^4v_3v_5$. Clearly, the magnitude of v_2 has a higher role to play in the latter than the former choice of the coefficients a_i. Hence, in the rest of this thesis, wherever relevant to the context, any general harmonic orders n_1, n_2 will be said to have the same importance in an SPC involving them, if we have $a_1=a_2$. On the same note, if $a_1>a_2$, then the importance of the harmonic n_1, in an SPC involving $n_1\psi_{n_1}$ and $n_2\psi_{n_2}$, will be said to be larger than that of n_2 and vice versa. The use of the terminology 'importance' is relevant because, if a harmonic n_1 is more important than n_2 in any SPC, then, the EbE fluctuations of the n_1 ordered anisotropy are going to play a larger role in determining the value of the SPC, than the EbE fluctuations of the n_2 ordered anisotropy.
Here, it must be pointed out that, the simplest SPCs involving anisotropy of order $2n$, that were pointed out in Chapter 5.1.1 and 5.1.2 inherently give a higher importance to the lower order harmonics in order to ensure rotational invariance. This is increases the usability of the SPCs in analyzing the dominance of the $2n$ ordered anisotropy in the system. This is because, the importance of ψ_2, for example being much more than that of ψ_{2n} in $\langle\cos(2n(\psi_{2n}-\psi_2))\rangle_{GE}$ would imply that this SPC can have a high value if and only if the dominant anisotropy is $2n$ and not otherwise. This limit gets better as n gets larger.

5.3 Geometrical Interpretation of PPCs

PPCs have a very similar geometrical interpretation as that of the SPCs, as we change the terminology from $v_n\rightarrow\epsilon_n$, $\psi_n\rightarrow\Phi_n$, and the azimuthal angles of final state hadrons satisfying cuts mentioned in Chapter 3.2 with azimuthal angles in configuration space of the nucleons participating in the collision. It will be of major advantage therefore, if the SPCs could estimate the PPCs, preferably in a linear way. That being the case, if the SPC of certain harmonic orders

gives high signals in a collision system, we could directly use it as a guide to inferring about its initial state geometry.
One major application of the above, can be found by investigating ^{16}O-^{16}O collisions. The ^{16}O nucleus is modeled to be having its nucleons clustered in a tetrahedron, with vertices being made up of four α particles [41]. If this is the case, then a way to probe it from high-energy experiments, would be by studying the SPCs that correspond to the different configurations of initial geometry. Further details are given in the Appendix (Chapter 6.2).

5.4 Centrality and Spherocity Dependence of SPCs

5.4.1 SPCs involving harmonic orders $n = 2, 3, 4, 5$

Shown in Fig. 4.1 is the SPC $\langle\cos(4(\psi_4 - \psi_2))\rangle_{GE}$. Considering only the SPC that is evaluated using events of all shapes, it is close to zero in the most central event classes, and then increases to a maximum in the mid-central event class, after which it starts decreasing. From the inferences laid out at the beginning of this chapter, it is understood that the occurrence of symmetry planes ψ_4 and ψ_2 are correlated in Pb-Pb collisions. The fact that $\langle\cos(4(\psi_4 - \psi_2))\rangle_{GE}$ when evaluated using the high-S_0 events in each centrality class is negative, and that its magnitude is similar to the SPCs of other event shape classes except for the most central class, points us towards the conclusion that, the role of EbE fluctuations is reflected well in this correlator - highest in the most central class and decreases towards the less central classes.
The SPC $\langle\cos(2\psi_2 + 3\psi_3 - 5\psi_5)\rangle_{GE}$ (Fig. 4.2) shows qualitatively same centrality dependence in all the different event shape classes. The fact that this SPC when evaluated using high-S_0 events does not show any strikingly different qualitative behavior, indicates that this particular correlation among ψ_2, ψ_3, and ψ_5 is free from the effects of EbE fluctuations. The fact that $\langle\cos(2\psi_2 + 3\psi_3 - 5\psi_5)\rangle_{GE}$ is neither equal, nor even close to zero, as well as positive in all centrality and event shape class, indicates that particle emission in the second, third and fifth order harmonics are well correlated, given equal importance to all of them (refer to Chapter 5.2).
Coming to the SPC $\langle\cos(2\psi_2 + 5\psi_5 - 3\psi_3 - 4\psi_4)\rangle_{GE}$ (Fig. 4.3), as its value, having considered only the high-S_0 events for its evaluation, fluctuates about zero across different centrality classes, this linear combination of symmetry planes is therefore dominated by EbE fluctuations. This is also illustrated by the fact that this SPC in the int-S_0 class is zero in the most central event class. Given also that all the harmonics appear with the same importance in this SPC, it can be concluded by looking at the centrality dependence of $\langle\cos(2\psi_2 + 5\psi_5 - 3\psi_3 - 4\psi_4)\rangle_{GE}$ that particle emission in the second, third, fourth and fifth order harmonics are correlated, but not as much as ψ_2, ψ_3 and ψ_5 are (Fig. 4.2), or as ψ_2 and ψ_4 are (Fig. 4.1). From this, the deduction that follows is, particle emission in fourth order anisotropy is not well correlated to that of the

third and fifth order anisotropies.
Coming to $\langle\cos(2\psi_2 + 4\psi_4 - 6\psi_3)\rangle_{GE}$ (Fig. 4.7), it is seen that there is an overlap of values across all event shapes within errors. Further, it is has very low magnitude in all centrality classes, and negative in all but the 50-60% centrality class. This crossing is only indicative that the particle emission in the second, fourth and third order anisotropies are decorrelated when giving third order anisotropy a greater importance. This is consistent with the fact that in a colliding system of Pb nuclei, anisotropies of co-prime orders need not have any correlation among them, as the collision region is almond shaped, and odd ordered anisotropies would be suppressed.

5.4.2 SPCs involving the Symmetry Plane ψ_6

Consider the SPCs $\langle\cos(6(\psi_6 - \psi_2))\rangle_{GE}$ and $\langle\cos(2\psi_2 + 4\psi_4 - 6\psi_6)\rangle_{GE}$, shown in Fig. 4.6 and Fig. 4.4 respectively. Both of them decrease slightly as we move from the 0-5% centrality class and then increase again as we move towards the mid-central event classes, for both integrated and the low S_0 event shape classes. This dip is also observed in the case of these SPCs being evaluated using low-S_0 events, but in a more enhanced way than in the case when these are evaluated using events of all shapes. This is indicative of the fact that the sixth order anisotropy is very highly affected due to EbE fluctuations of the final state particle distribution. This inference is supported by the fact that while ψ_2 and ψ_4 are well correlated (Fig. 4.1), the involvement of ψ_6 with an equal importance, in the SPC $\langle\cos(2\psi_2 + 4\psi_4 - 6\psi_6)\rangle_{GE}$, leads to the latter having values consistently lower than the former, only except for the most central event class. On the same note, $\langle\cos(6(\psi_6 - \psi_2))\rangle_{GE} < \langle\cos(2\psi_2 + 4\psi_4 - 6\psi_6)\rangle_{GE}$, when both are evaluated using events of all shapes, in each centrality class. This further emphasizes the inference that the particle emission in the second and sixth order anisotropies are not as correlated as they are in the case of emission in second and fourth order anisotropies.
Considering $\langle\cos(6(\psi_6 - \psi_3))\rangle_{GE}$, it can be seen that for the high-S_0 case, the value of the SPC increases again as we move from 0-5% to the 5-10% centrality class, supporting the inference from the last paragraph that ψ_6 is highly sensitive to EbE fluctuations in the Pb-Pb collision system. However, it is noteworthy that this SPC has roughly the same values within errors, across all event shape classes. In terms of the geometrical explanation provided at the beginning of this chapter, it is to be understood that the correlator $\langle\cos(6(\psi_6 - \psi_3))\rangle_{GE}$ is dominated by EbE fluctuations, and its non-zero values in all centrality classes are an artifact of the geometrical fact pointed out in Chapter 5.1.2.

5.4.3 SPCs that are Zero

The SPC $\langle\cos(6(\psi_3 - \psi_2))\rangle_{GE}$ is zero for all centrality and event shape classes, within errors, except for the 5-10% and the 50-60% centrality classes. In the central case (0-10%), the SPC

crosses zero twice. Given that second order anisotropy is more important in this SPC than the third order, it can be concluded, with support from the case of the SPC $\langle\cos(2\psi_2+4\psi_4-6\psi_3)\rangle_{GE}$, that particle emission in second and third order anisotropies are decorrelated in the Pb-Pb collision system. This has also been observed in experiment [21].
Coming finally to the SPC $\langle\cos(8\psi_2-3\psi_3-5\psi_5)\rangle_{GE}$, where the second order harmonic is more important, it is again seen to zero within errors, similar to the case of $\langle\cos(6(\psi_3-\psi_2))\rangle_{GE}$. Hence, it can be understood that when second order anisotropy is the dominant one in the Pb-Pb collision system, it has no correlation between particle emissions in third and fifth order anisotropies. It must be noted however, that this SPC alone cannot be used to conclude that ψ_2, ψ_3 and ψ_5 are decorrelated, because the simplest combination of these symmetry planes, where each order of anisotropy has an equal importance, shows a non-zero correlation among them. The only conclusion that can be drawn is that, as per AMPT, when processes being studied are such that they influence significantly only the second order anisotropy in a Pb-Pb collision, we can ignore their impact on the third and fifth order anisotropies.

5.5 Spherocity Independence of PPCs

In all the figures shown in Chapter 4, the right side plots indicate the PPCs corresponding to the SPCs which are shown on the left. In all of these plots (right side plots of Fig. 4.1 to Fig. 4.9), it can be seen that the PPCs are independent of the event shape classes - they all have overlapping values within error bars, across all centrality classes. This is to be understood from the fact that the event shape develops as a result of all the different stages of evolution of a collision of the Pb nuclei. Hence, a spherocity classification, does not change the value of PPCs. When initialization happens, only the overlap region of the colliding nuclei are going to play a role in the value of PPCs.

5.6 SPCs as a tool to study PPCs

5.6.1 Comparison of SPCs and PPCs

The PPCs which correspond to SPCs that are zero (Chapter 5.4.3), are more consistently close to zero, as they have low values and frequently cross the x-axis, as we move across centrality classes. An explanation similar to that in Chapter 5.4.3 applies immediately to the case of PPCs as well, where we only need to keep in mind that we are concerned with geometry of the spatial energy distribution of the colliding nuclei and not particle emission in the final state.
Further, considering the cases of the PPCs $\langle\cos(4(\Phi_4-\Phi_2))\rangle_{GE}$, $\langle\cos(2\Phi_2+3\Phi_3-5\Phi_5)\rangle_{GE}$, $\langle\cos(2\Phi_2+5\Phi_5-3\Phi_3-4\Phi_4)\rangle_{GE}$, $\langle\cos(2\Phi_2+4\Phi_4-6\Phi_6)\rangle_{GE}$, and $\langle\cos(6(\Phi_6-\Phi_3))\rangle_{GE}$, it can be seen from Fig. 4.1, Fig. 4.2, Fig. 4.3, Fig. 4.4 and Fig. 4.6 respectively, that the

SPCs follow qualitatively, the same centrality dependence as that of the PPCs from the most central to the mid-central event classes. After the mid-central classes, as we move towards the peripheral classes, we have that the participating nucleon distribution in the Pb-Pb collision system is highly anisotropic and has strong contributions from higher order anisotropies, which are not yet dampened out as a result of the several stages of evolution of the system, that are to come later on. This suggests towards the possibility of a linear relationship of the SPCs and PPCs, and the investigation of the same has been presented in Chapter 5.6.2.
Finally, it should noted that $\langle\cos(6(\Phi_6 - \Phi_2))\rangle_{GE}$ and $\langle\cos(2\Phi_2 + 4\Phi_4 - 6\Phi_3)\rangle_{GE}$, shown respectively in Fig. 4.5 and Fig. 4.7, have a strikingly different centrality dependence in comparison to their corresponding SPCs. $\langle\cos(6(\Phi_6 - \Phi_2))\rangle_{GE}$ goes on increasing sharply as we move from the most central to the less central classes, in contrast to $\langle\cos(6(\psi_6 - \psi_2))\rangle_{GE}$, which does not show as sharp a rise. The PPC $\langle\cos(2\Phi_2 + 4\Phi_4 - 6\Phi_3)\rangle_{GE}$ is positive and decreasing in its magnitude as we move from the most central to the less central event classes. The corresponding SPC, i.e., $\langle\cos(2\psi_2 + 4\psi_4 - 6\psi_3)\rangle_{GE}$, is negative and and close to zero. The deviation of these indicates the fact that if heavy-ion collisions evolve as modeled by AMPT, then the correlation between the sixth and the second order, and of the second and third order in the Pb-Pb collision system will be dampened.

5.6.2 Linear Relationship of SPCs to the PPCs

Observing the strikingly similar centrality dependence of the SPCs and the PPCs, which was pointed out in Chapter 5.6.1, it is very natural to see if the SPCs and PPCs have a linear relationship as modeled by AMPT. In order to test for this, the following quantity is defined:

$$R^{sp}_{(a_1,n_1),(a_2,n_2)\ldots(a_k,n_k)}([b]) = \frac{\langle\cos(a_1 n_1\psi_{n_1} + a_2 n_2\psi_{n_2} + \ldots + a_k n_k\psi_{n_k})\rangle_{GE,\,[b]}}{\langle\cos(a_1 n_1\Phi_{n_1} + a_2 n_2\Phi_{n_2} + \ldots + a_k n_k\Phi_{n_k})\rangle_{GE,\,[b]}} \tag{5.1}$$

The above is a ratio of the int-S_0 SPC to the PPC with harmonics $(n_1, n_2, ..., n_k)$ and coefficients $(a_1, a_2, ..., a_k)$, in a centrality class (denoted by $[b]$, as the impact parameter has been used for the centrality classification). For example, $R^{sp}_{(4,2),(1,-3),(1,-5)}$ has $a_1 = 4$, $n_1 = 2$, $a_2 = 1$, $n_2 = -3$, $a_3 = 1$, and, $n_3 = -5$.

$$\therefore\ R^{sp}_{(4,2),(1,-3),(1,-5)}[b] = \frac{\langle\cos(8\psi_2 - 3\psi_3 - 5\psi_5)\rangle_{GE,\,[b]}}{\langle\cos(8\Phi_2 - 3\Phi_3 - 5\Phi_5)\rangle_{GE,\,[b]}}$$

Fig. 5.2 shows the centrality dependence of these ratios for different choice of harmonics. The ratios of some of the SPCs and PPCs have not been considered, where either of them is close to zero for all centrality classes (discussed in Chapter 5.4.3 and 5.6.1), as such ratios would either diverge or be zero, as a consequence of which we cannot gain any insight into the relationship between these SPCs and their PPCs. All the ratios pointed out in Fig. 5.2 seem to have a plateau in the centrality range 10-50% with a slightly negative slope. In order to see how closely they can be approximated by a constant, the ratio of the standard deviation to the mean of the

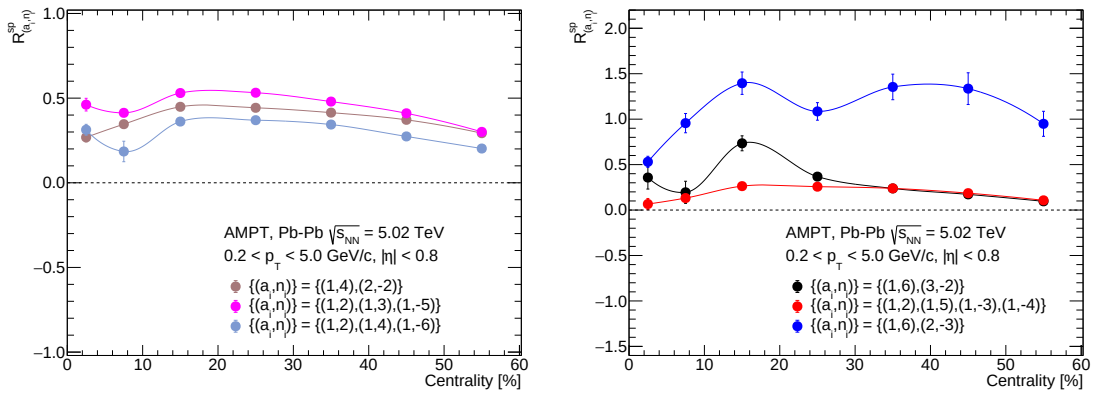

Figure 5.2: Centrality dependence of the ratios of int-S_0 SPCs to their corresponding PPCs, the choice of harmonics and their orders given in the legends.

$R^{sp}_{(a_1,n_1),(a_2,n_2),...,(a_k,n_k)}$ values in the 10-50% centrality classes is considered. Fixing a choice of harmonic orders and their importance, the mean and the standard deviation are defined as follows:

$$\mu = \frac{\Sigma_{r=1}^{4} x_r}{4} \qquad \sigma = \sqrt{\frac{\Sigma_{r=1}^{4}(x_r - \mu)^2}{3}} \tag{5.2}$$

where x_1, x_2, x_3, x_4 denote the values of the ratio in the 10-20%, 20-30%, 30-40% and 40-50% centrality classes respectively. The closer the value of σ/μ is to 0, the better is the approximation that the ratio of the SPC to PPC is constant. This in turn would imply that the particular SPC is linearly related to its corresponding PPC, i.e., they would have a similar behavior with centrality. As a second check, since a slightly negative slope with centrality is observed for most ratios (Fig. 5.2), we could fit the values of $R^{sp}_{(a_1,n_1),(a_2,n_2),...,(a_k,n_k)}$ as a linear function of the middle percentile of the centrality class, in order, using the least square fitting method. The better fits will be the ones which have higher values of R^2, defined as follows:

$$R^2 = 1 - \frac{\Sigma_{r=1}^{4}(x_r - X_r)^2}{\Sigma_{r=1}^{4}(x_r - \mu)^2} \tag{5.3}$$

In Eq. 5.3, x_r and μ are the same as in Eq. 5.2, and X_r are the predicted values of the fit, corresponding to x_r. $R^2 \to 1$ implies that the straight line fit is better. Now, using the fits which have R^2 close to unity, the ratios for which the straight line fit yields the least slope can be considered as the best estimator of PPCs among the others which have been investigated. Table 5.1 shows the values of the obtained parameters for different choices of harmonics and their importance.

As per the criteria of the lines with R^2 close to unity, the three SPCs that best estimate their corresponding PPCs linearly, are $\langle\cos(4(\psi_4 - \psi_2))\rangle_{GE}$, $\langle\cos(2\psi_2 + 3\psi_3 - 5\psi_5)\rangle_{GE}$ and $\langle\cos(2\psi_2 + 5\psi_5 - 3\psi_3 - 4\psi_4)\rangle_{GE}$. Considering however, the constant approximation of the SPCs, the best three which show a linear behavior to their corresponding PPCs are $\langle\cos(4(\psi_4 - \psi_2))\rangle_{GE}$,

$\{(a_i, n_i)\}$	$-m \times 10^3$	R^2	$\sigma/\mu \times 10^3$
(1,4),(2,-2)	2.80	0.9011	5.097
(1,6),(3,-2)	10.42	0.6376	26.49
(1,2),(1,3),(1,-5)	4.35	0.8615	11.59
(1,2),(1,4),(1,-6)	3.24	0.7207	9.805
(1,2),(1,5),(1,-3),(1,-4)	2.83	0.8307	9.042

Table 5.1: The first column gives the choice of harmonics (a_i, n_i) as they appear in $R^{sp}_{(a_i,n_i)}$. the second column gives the values of the slope m (rescaled by the mentioned factor) in the $y = mx + c$ fit of the values of the ratios against centrality using the least square error method, while the third column lists the parameter R^2 corresponding to this fit. The fourth column gives the σ/μ values (rescaled by the mentioned factor) of the approximation of the ratios to be a constant - equal their mean value.

$\langle\cos(2\psi_2 + 4\psi_4 - 6\psi_6)\rangle_{GE}$ and $\langle\cos(2\psi_2 + 5\psi_5 - 3\psi_3 - 4\psi_4)\rangle_{GE}$. Combining the conclusion from the two ways of fitting, we finally have that, as per AMPT, the SPCs $\langle\cos(4(\psi_4 - \psi_2))\rangle_{GE}$ and $\langle\cos(2\psi_2 + 5\psi_5 - 3\psi_3 - 4\psi_4)\rangle_{GE}$ are the best estimators of their corresponding PPCs in a system of Pb-Pb collisions at $\sqrt{s_{\rm NN}} = 5.02$ TeV.

Chapter 6

Summary and Outlook

6.1 Summary

The SPCs in the system of Pb-Pb collisions at $\sqrt{s_{\mathrm{NN}}}$ = 5.02 TeV provide rich insight into the geometrical properties of the distribution of final state particles. The S_0 based classification of the SPCs gives us a greater scope to study which correlators are influenced by event-by-event fluctuations as opposed to the case when the symmetry planes are actually decorrelated due to the geometry that develops as a result of the collision of the nuclei. Further, it has been observed that the SPCs qualitatively mimic the centrality dependence of the PPCs for most choices of harmonics and their importance. In addition, using the constant and the sloping straight line fits, the best SPCs have been identified which linearly predict the behavior of the PPCs in an AMPT like evolution of the Pb-Pb collision system at $\sqrt{s_{\mathrm{NN}}}$ = 5.02 TeV.

6.2 Outlook

It is clear from the entire study, that the SPCs provide a rich insight into the geometrical properties of a system. These will thus be useful to constrain the assumptions that go in to the modeling of a collision system. As an example, SPCs could be used to estimate PPCs which in turn would allow us to gauge the geometrical structure of the initial state of the colliding system. An application of this can be found, for example in ^{16}O-^{16}O collisions, to understand the role of α-clustering in the oxygen nuclei at high energies. This use case has been further elaborated in Appendix 6.2. Other uses involve model development by using Bayesian techniques to better constrain the parameters that go into event generation. Such studies are being conducted, and one can refer to [42] as an example.

Bibliography

[1] M. D. Schwartz, Cambridge University Press, ISBN 978-1-107-03473-0 (2014)

[2] https://tikz.net/sm_particles/

[3] S. Navas *et al.* [Particle Data Group], Phys. Rev. D **110**, 030001 (2024)

[4] B. R. Martin and G. Shaw, John Wiley & Sons, ISBN 978-0-470-03293-0 (2008)

[5] H. L. Anderson, E. Fermi, E. A. Long and D. E. Nagle, Phys. Rev. **85**, 936 (1952)

[6] https://www.osti.gov/servlets/purl/6524435

[7] D. H. Perkins, Cambridge University Press, ISBN 978-0-521-62196-8 (2000)

[8] M. A. Stephanov, PoS **LAT2006**, 024 (2006)

[9] W. Busza, K. Rajagopal and W. van der Schee, Ann. Rev. Nucl. Part. Sci. **68**, 376 (2018)

[10] R. Sahoo and T. K. Nayak, Curr. Sci. **121**, 1403 (2021)

[11] S. K. Das and R. Sahoo, Curr. Sci. **121**, 1156 (2021)

[12] C. Y. Wong, World Scientific Publishing Co. Pte. Ltd., ISBN 9810202636 (1994)

[13] N. Brambilla, M. A. Escobedo, J. Soto and A. Vairo, Phys. Rev. D **96**, 034021 (2017)

[14] S. Chatrchyan *et al.* [CMS], Phys. Lett. B **712**, 197 (2012)

[15] S. Acharya *et al.* [ALICE], Eur. Phys. J. C **84**, 813 (2024)

[16] J. Y. Ollitrault, Phys. Rev. D **46**, 245 (1992)

[17] S. Voloshin and Y. Zhang, Z. Phys. C **70**, 672 (1996)

[18] R. S. Bhalerao, M. Luzum and J. Y. Ollitrault, Phys. Rev. C **84**, 034910 (2011)

[19] C. Ding, W. Y. Ke, L. G. Pang and X. N. Wang, Chin. Phys. C **45**, 074102 (2021)

[20] M. Nahrgang, J. Aichelin, S. Bass, P. B. Gossiaux and K. Werner, Phys. Rev. C **91**, 014904 (2015)

[21] S. Acharya *et al.* [ALICE], Eur. Phys. J. C **83**, 576 (2023)

[22] S. Acharya *et al.* [ALICE], [arXiv:2409.04238 [nucl-ex]]

[23] B. Abelev *et al.* [ALICE], Phys. Rev. C **88**, 044909 (2013)

[24] N. Mallick, S. Tripathy, R. Sahoo and A. Ortiz, [arXiv:2001.06849 [hep-ph]]

[25] E. Cuautle, R. Jimenez, I. Maldonado, A. Ortiz, G. Paic and E. Perez, [arXiv:1404.2372 [hep-ph]]

[26] S. Prasad, N. Mallick, D. Behera, R. Sahoo and S. Tripathy, Sci. Rep. **12**, 3917 (2022)

[27] S. Prasad, N. Mallick, S. Tripathy and R. Sahoo, Phys. Rev. D **107**, 074011 (2023)

[28] A. Bilandzic, M. Lesch and S. F. Taghavi, Phys. Rev. C **102**, 024910 (2020)

[29] J. Jia and S. Mohapatra, Eur. Phys. J. C **73**, 2510 (2013)

[30] J. Jia, J. Phys. G **41**, 124003 (2014)

[31] D. Teaney and L. Yan, Phys. Rev. C **83**, 064904 (2011)

[32] Z. W. Lin, C. M. Ko, B. A. Li, B. Zhang and S. Pal, Phys. Rev. C **72**, 064901 (2005)

[33] X. N. Wang and M. Gyulassy, Phys. Rev. D **44**, 3516 (1991)

[34] M. L. Miller, K. Reygers, S. J. Sanders and P. Steinberg, Ann. Rev. Nucl. Part. Sci. **57**, 243 (2007)

[35] B. Zhang, Comput. Phys. Commun. **109**, 206 (1998)

[36] Z. w. Lin and C. M. Ko, Phys. Rev. C **65**, 034904 (2002)

[37] B. A. Li, C. M. Ko and G. Q. Li, [arXiv:nucl-th/9502047 [nucl-th]]

[38] G. L. Ma and Z. W. Lin, Phys. Rev. C **93**, 054911 (2016)

[39] C. Loizides, J. Kamin and D. d'Enterria, Phys. Rev. C **97**, 054910 (2018) [erratum: Phys. Rev. C **99**, 019901 (2019)]

[40] J. Adam *et al.* [ALICE], Phys. Rev. Lett. **116**, 222302 (2016)

[41] C. Ding, L. G. Pang, S. Zhang and Y. G. Ma, Chin. Phys. C **47**, 024105 (2023)

[42] M. Virta, J. Parkkila and D. J. Kim, [arXiv:2411.01932 [hep-ph]]

Appendix 1

Transverse Momentum

In the LHC, charged nuclei are accelerated upto energies that are roughly 10^3 times than their rest mass energies. The particles travel in collimated beams, and the collisions occur at interactions points designated across the LHC ring. Taking the momenta of the beam particles to be along the p_z-axis, the transverse momentum, is the projection of the momentum of a particle onto the $p_x - p_y$ plane. The choice of p_x and p_y can be done arbitrarily. Hence, in detectors, it is fixed as per the detector design. However, there is no such compulsion that an event must have its reaction plane aligned along the $p_x - p_z$ plane, which is why the rotation to such a frame was necessary in removing the effect of random event-by-event orientation of reaction plane, as was pointed out in Chapter 2.2. The mathematical definition of the magnitude of the transverse momentum however, is independent of any such rotation, and can be given by:

$$p_T = \sqrt{p_x^2 + p_y^2} \tag{6.1}$$

Pseudorapidity

In detectors, a convenient measurement of where a certain particle was detected can be provided by measuring the angular coordinates of the signal, with respect to the interaction point. These angular coordinates will be directly linked to the line of motion of the detected particle, which in turn is related directly to the final momentum components of the particle in the coordinate system of the detector. The polar angle of the momentum vector with respect to the p_z-axis, denoted by θ is given by:

$$\cos\theta = \frac{p_z}{p} \tag{6.2}$$

where p is the magnitude of the total momentum of the final state particle under concern. This polar angle is what is conveniently measured, and is used to define the quantity called pseudorapidity, denoted by η, defined as:

$$\eta = -\ln\left(\tan\left(\frac{\theta}{2}\right)\right) \tag{6.3}$$

Thus, instead of θ, experiments quote the value of η, and the angular coordinates are typically given by the $\eta - \phi$ space, where ϕ is the azimuthal angle of the transverse momentum, in the plane transverse to the beam axis, in the coordinate system of the laboratory. Further details of the usability of the pseudorapidity variable and other physical inferences that can be done by studying its spectrum can be found in the following reference - R. Sahoo, "Relativistic Kinematics," [arXiv:1604.02651 [nucl-ex]].

Appendix 2

Application of SPCs – ^{16}O-^{16}O Collisions

Given α clustering in ^{16}O nuclei, an ultra-relativistic collision between them would allow for three major configurations, as pointed out in Fig. 6.1. The left and the middle diagram in Fig. 6.1 depict the nuclear configuration if a head-on collision happens between two α-clustered ^{16}O nuclei, in eclipsed and staggered configurations respectively. If a ^{16}O-^{16}O collision occurs as shown in the left of Fig. 6.1, then the system would evolve with 3$^{\text{rd}}$ order anisotropy being dominant. In case the ^{16}O-^{16}O collision happens with nuclei in the middle configuration depicted in Fig. 6.1, then 6$^{\text{th}}$ order anisotropy will be dominant in the system that evolves. Hence, $\langle\cos(6(\psi_6-\psi_3))\rangle_{GE}$, being higher in ^{16}O-^{16}O collision than that of Pb-Pb in the most central event classes, could be an indicator of α clustering in ^{16}O.

Shown in the rightmost depiction of Fig. 6.1 is the case of mid-central collisions of two ^{16}O nuclei. The approach of nuclei is such, that any rotation about the beam axis would lead to a dominant 4$^{\text{th}}$ order and 2$^{\text{nd}}$ order anisotropy, accompanied by a weak 6$^{\text{th}}$ order anisotropy. Thus, a value of the SPCs $\langle\cos(4(\psi_4-\psi_2))\rangle_{GE}$, $\langle\cos(6(\psi_6-\psi_2))\rangle_{GE}$, and $\langle\cos(2\psi_2+4\psi_4-6\psi_6)\rangle_{GE}$ being higher in the ^{16}O-^{16}O than the Pb-Pb system in the mid-central event classes, could also act as a good indicator of α clustering in ^{16}O nuclei.

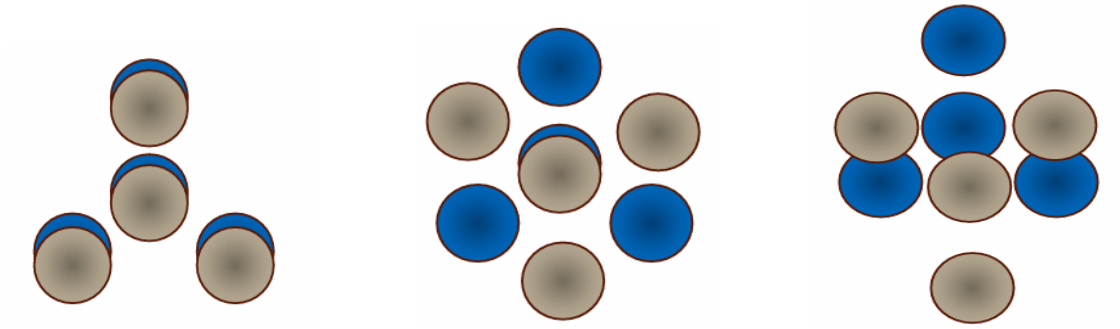

Figure 6.1: The possible initial configurations of two colliding ^{16}O nuclei. The circles represent the α particles and the colors indicate the α particles belonging to the different nuclei. In the left and the middle of the figure are the two possible configurations for most central collisions, while on the right is the case of mid-central collisions.

It is noteworthy here, that in order to confirm that it is indeed the sixth order anisotropy which is important in the most central case, we must investigate $\langle\cos(12(\psi_{12}-\psi_3))\rangle_{GE}$, to rule out the dominance of any $3k$ ordered anisotropy for an integer $k \geq 2$. Similarly, for the mid-central cases, $\langle\cos(8(\psi_8-\psi_2))\rangle_{GE}$ must be calculated, to check against any anisotropy higher than the 6^{th} order. The list of the SPCs discussed in this Appendix is supposedly exhaustive to point out a tetrahedral clustering in the ^{16}O nuclei, as rotations of any one of the nuclei in Fig. 6.1 in the most central cases, will only interchange the dominance of the 6^{th} and 3^{rd} order anisotropies, while in the mid-central case, it would the dominance of the 2^{nd} and the 4^{th} order anisotropies.